Ocean redox conditions between the Snowballs – geochemical constraints from Arena Formation, East Greenland

Eva L. Scheller, Alexander J. Dickson, Donald E. Canfield, Christoph Korte, Kasper K. Kristiansen, Tais W. Dahl

PII: S0301-9268(17)30383-2
DOI: https://doi.org/10.1016/j.precamres.2017.12.009
Reference: PRECAM 4954

To appear in: *Precambrian Research*

Received Date: 5 July 2017
Revised Date: 29 October 2017
Accepted Date: 3 December 2017

Please cite this article as: E.L. Scheller, A.J. Dickson, D.E. Canfield, C. Korte, K.K. Kristiansen, T.W. Dahl, Ocean redox conditions between the Snowballs – geochemical constraints from Arena Formation, East Greenland, *Precambrian Research* (2017), doi: https://doi.org/10.1016/j.precamres.2017.12.009

Ocean redox conditions between the Snowballs – geochemical constraints from Arena Formation, East Greenland

Eva L. Scheller[1,2], Alexander J. Dickson[3,6], Donald E. Canfield[4], Christoph Korte[5], Kasper K. Kristiansen[5], Tais W. Dahl[1*]

1) Natural History Museum of Denmark, University of Copenhagen, Øster Voldgade 5-7, DK-1350 Copenhagen K, Denmark

2) Division of Geological and Planetary Sciences, California Institute of Technology, 1200 E California Blvd, Pasadena, California 91125, USA

3) Department of Earth Sciences, University of Oxford, South Parks Road, Oxford, OX1 3AN, United Kingdom

4) Villum Professor, NordCEE and University of Southern Denmark, Campusvej 55, DK-5230 Odense M, Denmark

5) Institute of Geology and Natural Resources, University of Copenhagen, Øster Voldgade 10, DK-1350 Copenhagen K, Denmark

6) Department of Earth Sciences, Royal Holloway University of London, Egham, Surrey, TW20 0EX, United Kingdom

*Corresponding author, tais.dahl@snm.ku.dk (T. W. Dahl)

Abstract

The emergence of animal ecosystems is largely believed to have occurred in increasingly oxygenated oceans after the termination of the Sturtian and Marinoan glaciations. This transition has led to several hypotheses for the mechanism driving ocean oxygenation and animal evolution. One hypothesis is that enhanced weathering increased oceanic nutrient levels, primary productivity and organic carbon burial, and ultimately oxygenated the atmosphere and oceans. Another hypothesis suggests that an animal-driven reorganization of the marine biogeochemical cycles might have oxygenated the oceans. Through molybdenum (Mo), carbon (C), sulfur (S) isotopes and iron (Fe) speciation results from the Arena Fm, East Greenland, this study constrains ocean redox conditions during the Cryogenian, after the Sturtian deglaciation and before the major radiation of animals. Carbon and sulfur isotope stratigraphy is used to correlate the Arena Fm with other formations worldwide between the Sturtian and Marinoan glaciations (~720–635 Ma). The lower part of the Arena Fm (~25 m) consists of black shales deposited under locally euxinic conditions as evidenced by high proportions of highly reactive iron ($Fe_{HR}/Fe_T > 0.38$) and pyrite ($Fe_{PY}/Fe_{HR} > 0.7$). These black shales display small Mo enrichments (< 3 ppm) and low Mo/TOC compared to overlying shales and Phanerozoic euxinic sediments. The maximum δ^{98}Mo value is observed in the basal Arena Fm (1.5‰). Many samples display lower δ^{98}Mo than typical oceanic input fluxes, which can be explained by Mo isotope fractionation from a marine Mo pool with δ^{98}Mo ~ 1.3‰, similar to that inferred from other Cryogenic euxinic basins. The combination of low [Mo] and δ^{98}Mo suggests that widespread anoxia prevailed in the oceans at this time. Our data are consistent with most other studies from this time suggesting that ocean

oxygenation was not linked to Snowball Earth deglaciation, but was delayed until animals effectively entered the scene.

Keywords: Ocean oxygenation, Ocean anoxia, Neoproterozoic, Molybdenum, Molybdenum isotopes, stable isotope fractionation, Snowball Earth, Cryogenian

1. Introduction

The Cryogenian Period (~720–635 Ma) was host to two massive glaciation events; the Sturtian glaciation (717–660 Ma) and the Marinoan glaciation (<640 – 635.3 Ma) (Bold et al., 2016; Rooney et al., 2014)The Cryogenian also likely hosted the earliest metazoan ecosystems (Erwin et al., 2011). For example, the first possible sponge fossils are from 659–636 Ma (Maloof et al., 2010), and biomarker evidence also suggests that demosponges were present in the pre-Marinoan oceans (Love et al., 2009). These findings raise the question of whether climatic responses to the global glaciations could have produced a habitable environment for metazoans, for example in the form of pervasive ocean oxygenation (Scott et al. 2010; Sahoo et al. 2012; Planavsky et al., 2010; Kendall et al. 2015; Frei et al. 2009). Conversely, the evolving marine animal and algal ecosystems could also have caused ocean oxygenation (e.g., zooplankton; eukaryote-dominated phytoplankton; Brocks et al., 2017; Butterfield, 2009a, b; Canfield, 2014; Erwin, 2015; 2011; Lenton et al., 2014; Logan et al., 1995) or even dramatic climatic responses resulting in the global glaciations (Tzipermann et al., 2011).

In this study, we investigate marine redox conditions in the oceans during the Cryogenian warm interval as recorded in the rock record of the Arena Fm, East Greenland. At this time, metazoan ecosystems were still not abundant, and the Earth system relaxed from a long period of extreme cooling. Numerous other studies have explored ocean redox conditions from marine shales at this time, including the Datangpo Fm, South China (Feng et a., 2010; Li et al., 2012; Zhang et al., 2015), MacDonaldryggen Member of Elbobreen Fm, Svalbard (Canfield et al., 2008; Kunzmann et al., 2015), Tapley Hill, Australia, Twitya Formation (Sperling et al., 2016), NW Canada, and the Arena Fm, East Greenland (Canfield et al., 2008). These

data suggest that anoxic and ferruginous conditions prevailed on the continental shelves with anoxic and sulfidic (euxinic) conditions at other localities. A few studies have attempted to constrain the globally integrated ocean oxygenation state from uranium isotopes in carbonates of the Taishir Fm, Mongolia (Lau et al., 2017) and Mo isotopes in euxinic shales from the Black River Dolomite, Tasmania and the Datangpo Fm (Cheng et al., *this issue;* (Kendall et al., 2015). The molybdenum isotope composition of the euxinic shales suggest pervasive euxinia, whereas uranium isotopes in carbonates suggest that a short period of extensive ocean oxygenation followed the Sturtian glaciation before contracting towards a more anoxic ocean state during the Taishir anomaly (Lau et al., 2017). More constraints on the global oxygenation state and a better stratigraphic context are necessary to elucidate these discrepancies. Here, we provide chemostratigraphic data ($\delta^{13}C$, $\delta^{34}S$) together with local redox proxy data (Fe speciation, Fe/Al, Mo enrichments) and global redox proxy data ($\delta^{98}Mo$) from the Arena Fm, East Greenland.

The Mo isotope system is a useful proxy to decipher the globally integrated oxygenation state of the oceans. Mo is soluble in oxygenated seawater with a slow removal rate that gives its long residence time in the ocean (440 kyrs) and a globally uniform Mo isotope distribution in the oxic part of the oceans (Nakagawa et al., 2012; Miller et al. 2011; Kendall et al., 2017). This was probably also true in the Cryogenian where the predicted Mo residence time in the ocean, 100–200 kyr, was shorter than today, but still much greater than the oceanic mixing time scale (~1.5 kyr) (Dahl et al., 2011; Miller et al., 2011; Sarmiento and Gruber, 2006). Molybdenum is efficiently scavenged into euxinic sediments deposited under anoxic bottom waters with more than 11 µM hydrogen sulfide (H_2S), where molybdate is converted to reactive thiomolybdate anions. In hydrographically restricted situations

where the resupply of aqueous Mo from open-ocean seawater is slow, quantitative drawdown of Mo can subsequently occur, allowing the δ^{98}Mo of open ocean seawater to be recorded in the sediments (Neubert et al., 2008; Noordmann et al., 2015; Kendall et al., 2017). We discovered euxinic sediments near the base of the Arena Fm and applied the Mo isotope proxy to assess the global oxygenation state in the Cryogenian interglacial.

2. Geological settings

The Tillite Group (Cryogenian-Ediacaran) in East Greenland consists of five units, from below: Ulvesø, Arena, Storeelv, Canyon, and Spiral Creek formations. The Arena Fm (formerly Inter Tillite Beds) forms the interglacial unit between the two diamictite-bearing units Ulvesø and Storeelv (Stouge et al., 2011). Traditionally, the Tillite group has been correlated to the Polarisbreen Group in Svalbard based on comparable and substantial thicknesses of the lithological units in the two regions (Fairchild and Hambrey, 1995; Halverson et al., 2004). The Polarisbreen Group has been placed in a global chemostratigraphic context (mainly δ^{13}C and ^{87}Sr/^{86}Sr in carbonates) and assigned a post-Sturtian, pre-Marinoan age (Halverson et al., 2010; Kendall et al., 2006; Rooney et al., 2014).

Taken together, chemostratigraphic and lithological correlations point to a Sturtian age for the Ulvesø Fm and a post-Sturtian age for the Arena Fm. Chronostratigraphic age constraints from the Tillite group itself do not exist. Biostratigraphy, however, puts the Tillite Group in a Neoproterozoic context (Knoll and Swett, 1987; Vidal, 1976, 1979, 1981) with three characteristic acritarch taxa (*Bavlinella faveolata, Protosphaeridium laccatum* and *Trachysphaeridium timofeevi*) present in the Arena Fm. The first two taxa also occur in the Ulvesø diamictite. All of

these acritarchs occur in Tonian–Ediacaran strata around the world (Moczydlowska et al., 2017; Vidal, 1979). Chemostratigraphic data from the Tillite Group and the underlying Eleonora Bay Supergroup is also consistent with the Ulvesø and Storeelv formations representing glaciations of Marinoan and Sturtian age, respectively. Specifically, a deep negative carbonate $\delta^{13}C$ anomaly in bedgroup 19/20 below the Ulvesø Fm matches the Islay excursion in pre-Sturtian strata (~10 Myr) (Hoffman et al., 2012; Knoll et al., 1986; Kristiansen, 2007).

Palaeomagnetic studies of Bedgroups 18 and 19 in the Eleonore Bay Supergroup, found uncomformably below the Ulvesø unit, indicate a palaeolatitude of 3°S prior to the deposition of the Tillite group (Kilner et al., 2004; Mac Niocaill et al., 2008; Mac Niocaill et al., 2004). Paleogeographic reconstructions favor placing Greenland as the Southeastern marginal part of Laurentia (Li et al., 2008; 2013). The lithostratigraphic and chemostratigraphic correlations place East Greenland proximal to East Svalbard with a shared basin (Fairchild and Hambrey, 1995; Hoffman et al., 2012; Li et al., 2008). During the Marinoan glaciation, major rifting events had separated Laurentia from other continents (Li et al., 2013). Meanwhile, Greenland drifted progressively southward (Li et al., 2008; 2013).

The Arena Fm is exposed at several locations in East Greenland (Figure 1). It comprises 150–300 meters of carbonaceous mud- and siltstone with interbedded sandstone (Hambrey and Spencer, 1987). On Ella Ø, the formation is ~250 m thick, but incompletely exposed. Mud- and siltstone samples for geochemical analyses were collected from outcrops on Ella Ø exposed along the coastline at Bastionbugt (Figure 1). We collected 45 samples at ~2 m intervals in the section from three different exposures as two sizeable coverages (~59 and ~37 meters) obscured the stratigraphy at the sample site.

3. Methods

3.1 Carbon and sulfur contents and stable isotopes

3.1.1 Organic carbon contents

Samples were cut to remove surface contaminants, crushed in a shatterbox and crushed into a fine powder using an agate mill. Organic carbon contents were measured in ~1 g of homogenized rock powder treated with 3.2 M HCl, centrifuged, decanted, and centrifuged again with MQ water to remove all inorganic carbon. This process was repeated until a pH of 6 was reached in each sample solution. The residue was freeze-dried and then 300 mg was weighed into porcelain boats for carbon and sulfur analyses using an Eltra CS500 Carbon Sulfur Determinator at 1350 °C for 120 sec/sample calibrated against an in-house standard. The total organic carbon (TOC) contents obtained in this study were indistinguishable from a previous set of analyses at < 0.1wt% level (Table 1) (Kristiansen, 2007).

3.1.2 Carbon and oxygen stable isotopes

Carbon and oxygen stable isotopes were determined from the carbonate fraction (bulk carbonate), using freeze-dried and homogenized sediment samples; and from the organic fraction, using decarbonated samples. The carbonate analyses were undertaken at the University of Copenhagen using a continuous flow IsoPrime mass spectrometer equipped with a MultiFlow automated sample preparation system. Subsamples of bulk rock carbonate powders were weighed out (~0.6 mg pure carbonate) and placed into glass vials. Carbon isotopes were measured from the CO_2 that was liberated by dissolving the samples in phosphoric acid for 1 h at 70 °C (calcite) after the removal of atmospheric gases with He. Each batch of analyses included 50 samples and 10 internal standards (LEO Carrara marble; (see Ullmann et al., 2013 for further details). A separate set of sample powder were also run at 90°C

for 1 h to include dolomite $\delta^{13}C$ (Kristiansen, 2007). The carbon isotope analyses of organic matter were performed on dry residues after 1 h leaching with 10% HCl at 105°C (Kristiansen, 2007). Decarbonated powders (~50 µg pure organic carbon) was transferred into tin capsules and subsequently combusted in an Euro EA Elemental Analyzer. Generated CO_2 was transferred into the IsoPrime mass spectrometer and measured carbon isotope ratios were calibrated using the inhouse standard AK ($\delta^{13}C_{AK} = -25.3‰$). Results were expressed in per mille (‰) relative to the Vienna Pee Dee Belemnite (VPDB) standard.

After correction for linearity, reproducibility of $\delta^{13}C$ determinations was better than 0.1 ‰ (1 S.D.), whereas the uncertainty for $\delta^{18}O$ was better than 0.15 ‰ (1 S.D., n=10). All isotope ratio measurements were measured relative to the NBS-19 certified reference standard, and data is reported in δ-notation as parts per thousand (‰) deviation from the Vienna PeeDee Belemnite (V-PDB).

3.2 Sequential Fe extraction

Iron speciation analyses were performed using a calibrated sequential extraction procedure for fine-grained continental sediments (Poulton and Canfield, 2005). Total Fe concentrations were obtained from rock powders by first roasting sediments 8 h at 520°C, with subsequent digestion in 6 N HCl for 48 h (Aller et al., 1986). The concentrations of each iron pool were determined using a Perkin Elmer Atomic Absorpion Spectrometer AAS-100 at the University of Southern Denmark. The analytical error for each extraction was less than 5%. Pyrite sulfur was extracted by chromium digestion (Canfield et al., 1986; Zhabina and Volkov, 1978), trapped as Ag_2S, and its concentration determined gravimetrically with a reproducibility of ±5%.

3.3 Sulfur stable isotopes

Sulfur isotopic compositions were determined with a Thermo Analytical elemental analyzer, Flash EA 1112 series coupled via a ConFlo IV interface to a Thermo Delta V Plus mass spectrometer the University of Southern Denmark. The $^{34}S/^{32}S$ ratios are reported as $\delta^{34}S$ in terms of per mil relative to the Vienna Canyon Diablo Troilite (CDT) with analytical precision better than <0.3‰ (PACS-2, 1 SD = 0.3‰, n = 6 and in-house AgS_2, 1 SD = 0.15‰, n = 19).

3.4 Molybdenum concentrations and stable isotopes

Briefly, sample powders were accurately weighed and digested using inverse aqua-regia to extract all organic material and hydrogenous (seawater-derived) elements, following addition of a ^{97}Mo and ^{100}Mo enriched isotope spike. Molybdenum was separated from matrix elements using a single anion exchange procedure modified from Pearce et al. (2009) (Dickson et al., 2016). Molybdenum concentrations and stable isotopes were determined using a Nu-Plasma MC-ICPMS at Oxford University as described in detail in Dickson et al. (2016). $\delta^{98}Mo$ data are reported in $\delta^{98}Mo$ notation relative to NIST SRM 3134, where NIST 3134 is defined as 0.25‰ (Nägler et al., 2014). On this scale, modern seawater has $\delta^{98}Mo = 2.34\pm0.10$‰ (Goldberg et al. 2013). The long-term external reproducibility for $\delta^{98}Mo$ is ±0.08‰, as estimated from repeat digestions of the USGS SDO-1 shale standard (2 S.D., n = 31, average $\delta^{98}Mo = 0.79$‰). Mo concentrations were calculated by isotope dilution using the $^{100}Mo/^{95}Mo$ ratio.

3.5 Elemental data

Elemental data for Al, Ca, and Fe were collected using hand-held X-ray Fluorescence

(XRF) instrument Olympic DP-6000 at the University of Copenhagen. Loose ground powders were covered with 4.0 µm Prolene™ thin-film from Chemplex during analysis. Measurement time was 120 seconds for both heavy and light elements respectively. Samples were run with the reference standard PACS-3 before, during, and after analyses. XRF results were calibrated using method of Ahm et al. (2017). Estimated uncertainties (1SD) for Al, Ca, and Fe are 0.1-0.2 wt%, 1.8-1.9 wt%, and 0.1 wt%, respectively. Table 1 gives uncertainty estimates for each sample.

4. Results

4.1 Carbon and oxygen isotope composition of carbon

The lower part of the Arena Fm (375–390 m) shows a decreasing trend in $\delta^{13}C_{CARB}$ compositions from 1.4‰ to -4.5‰, reaching a constant minimum values of –5.1±1.5‰ (average ± 1 SD, n=9) for the rest of the section (Table 1, Figure 2). Similarly, $\delta^{18}O_{CARB}$ displays a decreasing trend (–3.8‰ to –14.1‰) in the lowermost section and constantly low values (-13.4±0.6‰, 1 sd, n=9) in the upper part of the section (Table 1, Figure 2). In contrast, $\delta^{13}C_{ORG}$ increases from –33.7‰ to –30.4‰ in the lowermost interval (Table 1, Figure 2).

4.2 Sulfur isotope composition of pyrite ($\delta^{34}S_{PY}$)

The sulfur isotope compositions of pyrites in the lower Arena Fm display a narrow range of high $\delta^{34}S_{PY}$ values (mean: 34±3‰, 1 sd, n= 10), whereas the upper part of the section shows larger $\delta^{34}S_{PY}$ variability from 10.8‰ to 64.8‰ (mean: 46±12‰, 1 sd, n=25) (Table 1 and Figure 3). All samples display values above that of the typical oceanic input (Phanerozoic values are <8‰; (Halevy et al., 2012), which is hard to

reconcile with the fact that pyrite formation is associated with the preferential removal of lighter isotopes relative to overlying seawater.

4.3 Total organic carbon (TOC) and total sulfur (TS).

Sedimentary TOC contents reach up to 3.0 wt% near the base of the Arena Fm (Figure 3). Thereafter, TOC contents systematically decrease up-section (374–390 m) reaching consistently low TOC values averaging 0.16±0.09 wt% at 400–550 m (1 SD, n= 26). The total sulfur content (TS) is higher in the lower part of the Arena Fm (mean: 2.5±0.6 wt%) than in the upper part of the section (mean: 0.6±0.7 wt%) (Table 1). The C/S (TOC/TS) weight ratios spans a wide range from 0.1 to 2.3 (mean 0.6±0.6) with no systematic stratigraphic trends (Table 1). The average C/S ratios are well below that of modern normal marine shales (= 2.8) and modern euxinic sediments (>2.8); and are comparable to Ordovician and Cambrian shales (0.5±0.1) (Raiswell and Berner, 1985a, b). The relatively low C/S values have previously been ascribed to the absence of terrestrial refractory organic material and the absence of bioturbation that would have enhanced pyrite preservation (Raiswell and Berner, 1985a).

4.4 Fe/Al

The Fe/Al ratios in the samples range from 0.6 to 1.6 with no discernable trends (Table 1, Figure 3). Importantly, the Fe/Al ratios remain above the 0.5 threshold indicative of sediment deposition in an anoxic marine basin (Lyons and Severmann, 2006). This result is robust despite the fact that samples taken from outcrop might have been affected by oxidative weathering. Fe/Al ratios are unaffected by the

carbonate dilution in samples deposited closest to the underlying Ulvesø diamictite that produce proportionally lower sedimentary Fe and Al contents (Table 1).

4.5 Sequential iron extraction (Fe_{CARB}, Fe_{OX}, Fe_{MAG}, Fe_{PY}, Fe_T)

The lowermost Arena Fm displays high $Fe_{HR}/Fe_T > 0.38$ characteristic of deposition in anoxic waters. The Fe_{HR}/Fe_T values systematically decline from 1.0 to ~0.3 in concert with Fe_{PY}/Fe_{HR} ratios from 0.9 to 0.1 (Table 1, Figure 3). The decline parallels that of the TOC profile. This indicates that the lower part of the Arena Fm was deposited under an anoxic and sulfidic water column (euxinic conditions). In five of the twelve studied samples, the Fe-carbonate content dominates the highly reactive Fe pool. These samples also stand out with extremely high carbonate content (Ca ~20 wt%) (Table 1). The upper part of the Arena Fm (400–550 m) displays lower Fe_{HR}/Fe_T ratios oscillating between ~0.2 and ~0.5 with no discernable trends. On average, the highly reactive iron phases comprise of pyrite (38%), magnetite (32%), Fe-carbonates (19%) and a to a lesser extent Fe(III) oxides (12%) (Table 1). Importantly, Fe_{PY}/Fe_{HR} ratios remain below the euxinic threshold (0.7–0.8) although a few high values near the euxinic threshold occur at 554 m.

4.6 Mo, Mo/Al and Mo/TOC

Sedimentary Mo contents decline from 3.2 ppm (375 m) to 0.2 ppm (392 m) in the lowermost Arena Fm (Table 1, Figure 3). These concentrations are well below that of modern euxinic marine sediments (30–200 ppm), average Proterozoic shales (24 ppm) and contemporaneous euxinic shales deposited in the Datangpo Fm, South China (~5-30 ppm) (Dahl et al., 2013; Li et al., 2012; Scott and Lyons, 2012; Scott et al., 2008). In the upper part of the section, sedimentary Mo contents are variably low, 0.1 to 0.6

ppm; well below that of average upper continental crust (which is ~1.5 ppm; Taylor and McLennan, 1995), but not atypical of iron oxide rich sediments (e.g. jasper bands, Baldwin et al., 2013).

The Mo/Al ratios in the lower part of the Arena Fm range from 0.10–0.82 with 6 out of 8 samples having a higher Mo/Al than riverine particulates (0.32), average continental crust (0.19) and sediments from the upper part of the Arena Fm (0.04±0.02, n=5). Using Al as a tracer for detrital input, we calculate that authigenic Mo accounts for at least ~1.5 ppm or ~65% (assuming detrital Mo/Al = 0.19), and perhaps up to ~3 ppm or 95% Mo in the lower Arena Fm (assuming detrital Mo/Al = 0.04) (Martin and Meybeck, 1979; Taylor and McLennan, 1995).

The Mo and TOC content in the euxinic Arena shales are linearly correlated with a slope of 1.3±0.3 ppm/wt% (1 SD, Figure 6). The average Mo/TOC ratio in the Arena shales is 1.9±1.0 ppm/wt% (1 SD, n = 11) with no clear stratigraphic trends. This is well below the average of Proterozoic shales (6.4 ppm/wt%) (Scott et al., 2008). However, one sample in the upper Arena Fm at 537 m is a single outlier that contains particularly low TOC content and 7.8 ppm Mo giving a Mo/TOC ratio of 24.5 ppm/wt%.

4.7 Molybdenum isotope composition (δ^{98}Mo)

The δ^{98}Mo profile shows a systematic decline upsection with values ranging from +1.47‰ to –0.26‰ in the lower part of Arena Fm (Table 1, Figure 3). The δ^{98}Mo values in the upper part are low and more variable at +0.12 to –0.86‰. These δ^{98}Mo values are characteristically below that of average crustal rocks (~0.3‰) and average oceanic input (~0.7‰), implying that Mo isotope fractionation occurred during transport from the crustal source to the sediments (Figure 4) (Kendall et al., 2017).

In a plot of δ^{98}Mo vs 1/Mo (Figure 4), it is clear that binary mixing between a Mo detrital source and an authigenic component does not explain all the chemical variability. However, δ^{98}Mo and Mo/Al display a positive correlation in the lowermost part of the Arena Fm. From this, we infer that sediments of the lower Arena Fm contain an authigenic Mo component with high δ^{98}Mo and modest Mo enrichments mixed with a very low δ^{98}Mo and variably low Mo component. In addition, another authigenic component of Mo-depleted material with a negative δ^{98}Mo value could contribute to the variability observed in the upper Arena shales. Assuming the detrital component in the lower Arena Fm has a composition similar to the average of bulk samples in the upper part of the Arena Fm; *i.e.*, $(Mo/Al)_{detr}$ = 0.04±0.02 (1 SD, n=5) and $\delta^{98}Mo_{detr}$ = –0.45±0.42‰ (1 SD, n=5), we estimate the Mo isotope composition of the "high Mo" authigenic component by subtracting the detrital component:

$$\delta^{98}Mo_{AUTH} = [\delta^{98}Mo - (1-f_{auth}) \cdot \delta^{98}Mo_{detr}]/f_{auth} \qquad \text{(equation 1)}$$

where $f_{auth} = 1 - (Mo/Al)_{detr}/(Mo/Al)$.

Our data shows that $\delta^{98}Mo_{AUTH}$ systematically declines up-section with the highest values in the lower Arena Fm at 1.57±0.06‰ to -0.53±0.06‰. Uncertainty estimates for $\delta^{98}Mo_{AUTH}$ represent propagated errors assuming the variables in equation 1 are independent.

5. Discussion

5.1 The age of the interglacial deposits in East Greenland

Chemo- and lithostratigraphic correlations provide an age of the Arena Fm suggesting

the Ulvesø and Storeelv diamicties are of Sturtian and Marinoan age, respectively (Hoffman et al., 2012; Fairchild et al., 2016). Previous chemostratigraphic studies mainly focused on the Polarisbreen Group of NE Svalbard (Halverson et al., 2004; Hoffman et al., 2012; Fairchild et al., 2016) although Kristiansen (2007) provided $\delta^{13}C$ data for the Tillite Group and Eleonore Super Group. A negative $\delta^{13}C$ anomaly is recorded in the pre-glacial Bedgroup 19/20 (Kristiansen, 2007; Stouge et al., 2011). Early studies attributed this excursion to the late Cryogenian Trezona anomaly implying that the Sturtian glaciation is not preserved in East Greenland (Halverson et al., 2004; Kristiansen, 2007; Stouge et al., 2011). In these models, the MacDonaldryggen Mb and Arena Fm formed as part of the same basin during the Marinoan glaciation by meltwater plumes underneath an ice-covered ocean (Halverson et al., 2004). However, the more recent recognition of the Islay negative anomaly in pre-Sturtian (Tonian) strata worldwide has led to a re-assessment of the negative $\delta^{13}C$ anomaly in Bedgroup 19/20, supporting a Sturtian age of the Ulvesø Fm (Halverson et al., 2010; Hoffman et al., 2012). Given that the Storeelv diamictite represents the Marinoan ice age as determined in Hoffman et al. (2012), the Arena Fm must have been deposited during the Cryogenian warm interval (Halverson et al., 2010; Hoffman et al., 2012; Fairchild et al., 2016). The $\delta^{13}C$ and $\delta^{34}S$ data provided in this study are consistent with this view, as explored below.

5.1.1 Characteristically extreme $\delta^{34}S$ values in pyrite

The sulfur isotope composition of marine pyrites, $\delta^{34}S_{PY}$, rarely exceeds average Phanerozoic oceanic input (<8‰) (Halevy et al., 2012) simply because pyrite is the major sink for reduced sulfur that preferentially removes the lighter sulfur isotopes from the marine sulfate reservoir (Canfield, 2004). Nevertheless, several Cryogenian

interglacial deposits including MacDonaldryggen Fm, Datangpo Fm, Aralka Fm, Twitya Fm, and Tapley Hill Fm display extremely heavy values, at ~30–60‰, similar to those observed in the Arena Fm (Feng et al., 2010; Li et al., 2012; Ries et al., 2009). Although extremely heavy pyrite $\delta^{34}S$ values are not a worldwide signature in the ocean (e.g. Oman), it is clear that an extremely sulfate-depleted ocean is required to achieve these values (Ries et al., 2009). This property is typical, although not unique, for the Cryogenian warm interval oceans (e.g. Nama Group, 549–545 Ma) (Gorjan et al., 2000; Ries et al., 2009). Therefore, the $\delta^{34}S$ data in the Arena Fm is consistent with previous chemo- and lithostratigraphic correlations.

5.1.2 $\delta^{13}C_{CARB}$ profile of the Arena Fm

Several lines of evidence suggest that the $\delta^{13}C_{CARB}$ profile in the Arena Fm shales is not representative of contemporaneous seawater due to the negligible carbonate content, its potentially authigenic origin and/or diagenetic overprint. The negative $\delta^{13}C_{CARB}$ trend from +1.4 to –4.5‰ in the lower Arena Fm is not coupled to changes in $\delta^{13}C_{ORG}$ as would be expected if both carbonates and marine biomass precipitated from seawater, Figure 2. The observed $\delta^{13}C_{CARB}$ profile is distinct from the Neoproterozoic $\delta^{13}C_{CARB}$ record as it does not exhibit the Taishir anomaly or the high +8‰ plateau observed both before and after the Taishir excursion (e.g., Johnston et al., 2012; Lau et al., 2017). However, the Arena Fm could represent a temporal interval distinct from the Taishir Fm.

The inorganic carbon content (0.35±0.37 wt%) is generally low in the upper Arena Fm, Table 1. The low carbonate content is at least compatible with a contribution of authigenic carbonate derived from anaerobic respiration processes that boost alkalinity to the point where carbonate minerals form inside the sediment pore

fluids. This process would produce markedly lower $\delta^{13}C_{CARB}$ values than contemporaneous seawater. Alternatively, the trend could arise from extensive diagenetic overprint generated by oxygen from meteoric water and dissolved inorganic carbon derived from oxidation of organic matter affecting carbonate-lean samples the most (Irwin et al., 1977; Knauth and Kennedy, 2009; Derry, 2010; Swart, 2015) (Figure 5). This could explain why negative $\delta^{13}C_{CARB}$ trend in the lower Arena Fm is correlated to a negative $\delta^{18}O_{CARB}$ trend (Fig. 2) and samples with up to 20 wt% carbonate tend to show higher $\delta^{13}C_{CARB}$ values. Further, a comparison of $\delta^{13}C_{CARB}$ values in dolomite and calcite from the same samples (Kristiansen, 2007) versus $\delta^{13}C_{CARB}$ in mainly the calcite fraction of the Arena shales (this study) suggest that the dolomitic component carries the most altered $\delta^{13}C_{CARB}$ signatures (negative $\delta^{13}C_{CARB}$ offset by 0.1–3.9‰). These features can be explained if the dolomitizing fluids also carried relatively ^{13}C- and ^{18}O-depleted signatures (Swart, 2015).

If secondary alteration induced the negative $\delta^{13}C_{CARB}$ trend observed in the lower Arena Fm, then the positive $\delta^{13}C_{ORG}$ trend (from –34‰ to –30‰) could be interpreted in two ways. Firstly, $\delta^{13}C_{ORG}$ could record a positive carbon isotope trend in the global exogenic carbon cycle. Global chemostratigraphic correlations shows a $\delta^{13}C_{CARB}$ increase from –4‰ to +8‰ both in the aftermath of the Sturtian glaciation and during the rising limb of the negative Taishir anomaly (Halverson and Shields-Zhou, 2011; Halverson et al., 2010). In both cases, the lower Arena Fm would represent a short period during the early Cryogenian warm interval either before the Taishir anomaly (662.9±4.3 Ma to 657.2±6.9) or as part of the Taishir anomaly (between 657.2±6.9 to 654.5±3.8) (Bold et al., 2016). This timing would imply extreme sedimentation rates an order of magnitude higher (~180 m/My) than typical for shales (Einsele, 2013), which may be realistic during the retreat of the Sturtian ice

cover.

Alternatively, the $\delta^{13}C_{ORG}$ profile could also have been decoupled from secular changes in seawater $\delta^{13}C$, for example as a result of a shift in the magnitude of isotope fractionation in response to an ecological shift and/or change in the pathway for organic matter export to the sediments. If so, then the Arena Fm could well have been deposited during the entire interglacial interval from ~663 to 636 Ma at a typical sedimentation rate for shales (Bold et al., 2016).

5.2 Local redox conditions in the Arena basin

The local redox conditions in the Arena basin are similar to several other anoxic basins during the Cryogenian interglacial, namely MacDonaldryggen Mb, Datangpo Fm, Twitya Fm and Black River Dolomite (Feng et a., 2010; Li et al., 2012; Zhang et al., 2015; (Canfield et al., 2008; Kunzmann et al., 2015). Anoxic and non-sulfidic (ferruginous) bottom water conditions have been inferred for the MacDonaldryggen Member and the Twitya Fm (Canfield et al., 2008; Kunzmann et al., 2015), whereas the Black River Dolomite are consistently euxinic (Kendall et al., 2015) and the lower part of the Datangpo Fm were deposited under euxinic and/or ferruginous conditions (Feng et al., 2010; Li et al., 2012; Cheng et al., *this issue*).

The Fe speciation and Fe/Al data constrain redox conditions in the bottom waters of the local marine depositional environment. Highly reactive Fe phases, Fe_{HR}, comprise carbonates (Fe_{CARB}), ferric oxides (Fe_{OX}), magnetite (Fe_{MAG}), and pyrite (Fe_{PY}) that characteristically exceed 38% of the total iron, $Fe_{HR}/Fe_T > 0.38$, in marine settings with anoxic bottom waters. Lower Fe_{HR}/Fe_T ratios may suggest oxic conditions, although high depositional rates of detrital material also produce deceptively low

Fe_{HR}/Fe_T (Poulton and Raiswell, 2002; Raiswell and Canfield, 1998). The Fe_{PY}/Fe_{HR} ratio distinguishes between an anoxic, non-sulfidic (potentially Fe^{2+} containing) water column and a sulfidic water column (Poulton and Canfield, 2011). Sediments deposited under anoxic and sulfidic (euxinic) waters contain high Fe_{Py}/Fe_{HR} ratios above ~0.7 for Phanerozoic sediments (Anderson and Raiswell, 2004; März et al., 2008).

Fe speciation data in the lower Arena Fm (375–390 m) imply predominantly euxinic conditions (Figure 6). However, euxinic samples are interbedded with five samples with $Fe_{Py}/Fe_{HR}<0.7$ in which Fe-carbonate dominates the highly reactive Fe pool (Figure 6). These five samples all display low Al (1.5–4.7 wt%), high Ca (9.7–21 wt%), high total carbon contents (4.3-10.5 wt%), and high Fe_{CARB} (0.7-2.9 wt%) (Figure 6). These features suggest inorganic carbonate precipitation with prevalent Fe substitution. The temporal regularity of these interbedded samples suggests cyclical precipitation events. It is likely that such surges in precipitation of carbonates radically augmented sedimentation rates in those temporal intervals (Clarkson et al., 2014). Therefore, we infer that the lower Arena Fm (375–390 m) represents a primarily euxinic environment.

In the upper Arena Fm, Fe_{HR}/Fe_T values are close to the 0.38 threshold (0.36–0.48) suggesting that either oxic or anoxic/ferruginous bottom water conditions prevailed in the basin (Figure 6). All samples of the Arena Fm display higher Fe/Al ratios (0.93±0.36) than average shales and average river-suspended particulates (0.5–0.56). The upper Arena Fm is also substantially enriched (Fe/Al = 0.86±0.19) indicative of ferrous iron transport within anoxic bottom waters of the Arena basin. However, the Arena shales display a lower Al/Ti mass ratio (14.9±3.7) than average upper continental crust (24.8), and are more similar to mafic rocks of the Franklin

Large Igneous Province (Al/Ti = 8-20) with higher Fe/Al mass ratio (0.8–1.5). This observation suggests that the detrital component in the Arena shales could contain higher Fe/Al than typical upper continental crust sediments (Cox et al. 2015; Cox, 2015; Dostal et al., 1985; Wedepohl, 1995). In combination with the muted Fe_{HR}/Fe_T = 0.30±0.11 enrichments (this study) and limited Fe isotope fractionation in bulk rock samples from MacDonaldryggen and Arena Fm, we suggest that the detrital Fe component overwhelmed any shelf-to-basin reactive iron shuttle (Kunzmann et al., 2017a). Therefore, the Fe-based proxies are not decisive for the upper Arena Fm and it could have been deposited either in oxic settings or under anoxic/ferruginous bottom waters with a mafic detrital component.

5.3 Basinal restriction

Today, the Mo scavenging process gives rise to Mo-TOC co-variation in euxinic sediments with slopes between ~5 and ~45 depending on water exchange between the basin and the open ocean. The highly restricted Black Sea, for example, yields 9-fold lower Mo/TOC ratios than the more open setting of the Saanich Inlet (Algeo and Lyons, 2006). The observed Mo/TOC slopes in the euxinic Arena shales, at 1.3±0.3 ppm/wt%, are substantially lower than observed for any modern euxinic setting (Figure 7), indicative of either an extremely restricted basin and/or lower Mo availability in the Cryogenian oceans. The Mo/TOC slope is similar to that of ~ 640 Ma organic mudrocks of the Black River Dolomite in Tasmania (mean: 3.5±1.1 ppm/wt%, 1 SD, n=10; Kendall et al., 2015) and 3 to 15-fold lower than in the ~ 663–654 Ma Datangpo sections, implying that the Arena Fm and the Black River Dolomite were deposited in more restricted basins (Cheng et al., *this issue*). However, the Greenland-Svalbard basin was laterally extensive, contained characteristic marine

acritarchs, with strontium isotope compositions matching similar age marine carbonate deposits (Halverson et al., 2004; Hoffman et al., 2012; Kunzmann et al., 2015; Fairchild et al., 2016). Therefore, we infer that the Greenland-Svalbard basin, although restricted, still exchanged seawater with the open ocean.

Importantly, Mo enrichments are also low in euxinic sediments from the more open-marine euxinic Datangpo basin (~30 ppm) relative to modern open-shelf euxinic settings (~130 ppm) suggesting ~4-fold lower Mo concentration in the Cryogenian ocean than today (Cheng et al., this issue; Li et al., 2012). The markedly lower Mo concentrations in the Arena Fm (0.1–7.8 ppm), even compared to the Datangpo Fm, could indicate that hydrogen sulfide levels in the basal Arena Fm (375–390 m) were too low for efficient conversion of molybdate to reactive thiomolybdate. We note that some sulfidic sediments deposited under oxic waters do produce Mo-TOC co-variation with a shallow slope similar to the Arena Fm (Brucker Poulson et al. 2009). Therefore, we cannot rule out that low sedimentary Mo/TOC was produced in euxinic basins where bottom water H_2S concentrations never exceeded the 11 µM threshold.

5.4 Reconstructing global redox conditions

The marine Mo isotope budget varies as a function of the global ocean oxygenation state. The major source of oceanic Mo is in the form of MoO_4^{2-} via rivers with an average δ^{98}Mo value of 0.7 ‰ (Archer and Vance, 2008). In oxygenated waters, molybdenum isotope fractionation occurs when Mo is adsorbed onto Mn-oxides resulting in an isotopic difference of -3‰ between the Mn-oxide containing sediments and seawater. In euxinic settings where H_2S concentrations exceed 11 µM and Mo is converted to reactive thiomolybdate ions ($MoO_{4-x}S_x^{2-}$), molybdenum may be quantitatively removed with no net isotopic difference expressed between the

sediments and seawater source (e.g. see Kendall et al., 2017 for a recent review). Another important Mo sink is settings of intermediate redox conditions, where Mo is eventually captured by H_2S inside sedimentary pore fluids. Under these conditions Mo adsorption onto Fe-oxides, such as ferrihydrite, hematite, magnetite, and goethite, in the oxic zone followed by reductive dissolution may contribute to a variable and smaller isotope offset from seawater; *e.g.,* ~0.8‰ (Poulson Brucker et al. 2009; Goldberg et al., 2012). Isotope fractionation between sediments and seawater always cause preferential removal of isotopically lighter Mo isotopes leaving the modern ocean with a uniform and isotopically heavy δ^{98}Mo composition of 2.34±0.10 ‰ (Kendall et al., 2017).

Euxinic sediments have the potential to record the δ^{98}Mo isotope composition of penecontemporaneous ocean seawater and constrain the globally integrated extent of Mo-sulfide removal into seafloor sediments (Arnold et al., 2004; Dahl et al., 2011). Effective transfer of seawater δ^{98}Mo values into the sedimentary rock record depends on enough hydrogen sulfide available for quantitative thiomolybdate formation in the local basin, and on hydrographic conditions that allow enough time for quantitative removal to occur (Dahl et al., 2010a; Neubert et al., 2008). Currently, no independent control measures can be taken to ensure that a sedimentary rock captures the 'seawater' value (Dahl and Wirth, 2017). Molybdenum isotope fractionation occurring in the local basin produces sediments with lower δ^{98}Mo than overlying seawater. Therefore, the highest δ^{98}Mo value in a section is typically used as a minimum estimate of seawater δ^{98}Mo (Dahl et al., 2010b), but we can also assess seawater δ^{98}Mo if we understand the magnitude of Mo isotope fractionation associated with sediment burial in the Arena Basin. We explore both of these

approaches further below.

5.4.1 Mo-isotope fractionation throughout Arena Fm

The highest δ^{98}Mo value in the Arena Fm is 1.5‰, occurring in euxinic sediments close to the Ulvesø (Sturtian-age) tillite. Therefore, this is a lower estimate of seawater δ^{98}Mo at this time in the post-Sturtian oceans. Several of the euxinic samples in the lower part of the Arena Fm carry authigenic Mo enrichments with much lower δ^{98}Mo values (> –0.53‰) than the oceanic Mo inventory can achieve as a whole (≥0.7‰) (Kendall et al., 2017). Hence, Mo isotope fractionation occurred most of the time when dissolved Mo was transported into the Arena basin and/or within it. Indeed, we also know that local Mo isotope fractionation must have taken place when bottom water H_2S levels dropped below the threshold of thiomolybdate formation during the transition from euxinic to ferruginous conditions in the Arena basin. At this time, δ^{98}Mo systematically decreased from 1.47‰ to –0.26‰. Thus, decreasing bottom water H_2S would imply that molybdate conversion to thiomolybdate was incomplete and that another Mo burial pathway took over or even dominated while conditions were still (perhaps mildly) euxinic.

The upper Arena shales display low and variable δ^{98}Mo isotope compositions (0.12‰ to –0.86‰) and very low sedimentary Mo contents that we ascribe to Mo burial associated with Fe-oxide precipitation in an anoxic and ferruginous environment. Molybdenum adsorbs onto magnetite, ferrihydrite, goethite, and hematite with distinct magnitudes of isotopic differences at 0.83±0.60‰, 1.11±0.15‰, 1.40±0.48‰, and 2.19±0.54‰ respectively (Goldberg et al., 2009). We propose that Mo co-precipitated with ferrihydrite ($Fe_2O_3 \cdot 0.5H_2O$) from the water column and subsequently re-dissolved in the sediment pore fluids, before some fraction was captured in magnetite,

goethite, pyrite, and Fe-carbonate during early diagenetic Fe reduction. Hematite is not a product of early diagenesis and formed later. Molybdate ions (MoO_4^{2-}) from seawater were also delivered by diffusion into the pore fluids, where Mo fixation in insoluble Fe phases took place. This process would only dilute the isotopic offset between the sediments and the open ocean. Ultimately, the maximal isotopic difference between sediments and the seawater source also depends on how large a proportion of Mo is escaping back into the water column by diffusion (Clark & Johnson, 2008). The diagenetic Mo capture efficiency in the sediments depends on 1) the depth at which the Mo-shuttle (e.g. ferrihydrite) dissolves and liberates Mo back to interstitial pore-spaces, 2) the depth at which Mo re-precipitates with other Fe oxide phases (e.g. magnetite/goethite/pyrite/Fe-carbonate) and 3) the Mo affinities of the involved mineral phases, and 4) the availability of Mo surface sites on the final host phase. For example, we expect little diffusional Mo loss if ferrihydrite dissolution occurs deep inside the sediments, fresh Fe oxides immediately form at the same depth, and there are plenty of surface sites available for Mo capture in the sediments. In this situation, essentially all Mo will be captured in the magnetite/goethite/pyrite/Fe-carbonate inside the sediments and there will be no further isotope fractionation associated with the final Mo fixation step. Alternatively, if ferrihydrite dissolves near the sediment-water interface and Mo is liberated in the form of MoO_4^{2-}, and another reactive Fe phase instantaneously forms, then we expect approximately half of the Mo (e.g. the fraction that diffuses in a downwards direction) to be eventually incorporated into freshly formed insoluble Fe phases, whereas the rest is lost to the water column. In this case, the magnitude of isotope offset between sediment and dissolved MoO_4^{2-} in the pore fluids will be ~half of the isotope discrimination between reactant and products; that is -0.41±0.30 to -0.70±0.24‰ for

magnetite and goethite, respectively. Adding the isotope fractionation associated with ferrihydrite precipitation, we calculate that sediments would carry variable δ^{98}Mo values that are maximally between 1.52±0.45‰ and 1.81±0.39‰ below that of contemporaneous seawater (calculations: 1.11±0.15‰ + 0.41±0.30‰ and 1.11±0.15‰+ 0.70±0.24‰). Hence, both the absolute δ^{98}Mo values and the variability between samples in the ferruginous Arena shales, at –0.45±0.42‰, are fully explained by differences in the Mo removal pathway within the Arena basin and open ocean seawater at a constant steady state δ^{98}Mo value between 1.07±0.61‰ and 1.36±0.57‰ (calculations –0.45±0.42‰+1.52±0.45‰; –0.45±0.42‰ + 1.81±0.39‰).

Clearly, this estimate is uncertain in part because we do not know the exact Mo burial pathway, or the efficiency of Mo sequestration during early diagenesis and because the magnitude of Mo isotope fractionation during pyrite and Fe-carbonate precipitation in pore fluids are also not known. Nevertheless, our model and calculations demonstrate that Cryogenian seawater may well have had δ^{98}Mo similar to earlier Neoproterozoic oceans (in contrast to the view held in Baldwin et al. 2013), and we conclude that seawater δ^{98}Mo was most likely well below that of the modern ocean.

5.4.2 Estimating the globally-integrated ocean oxygenation state, ~660–636 Ma

The lower Arena Fm contains a maximum δ^{98}Mo composition of ~1.5‰, and we provide a model-dependent and more uncertain estimate that the upper part of the Arena Fm was deposited with seawater value of δ^{98}Mo = 1.1-1.3‰ (±0.6‰). The contemporaneous lower part of the euxinic Datangpo Fm and the Black River Dolomite display maximal δ^{98}Mo values at ~1.1‰ (Kendall et al., 2015; Cheng et al.,

this issue). Hence, the best estimates for the δ^{98}Mo value for the Cryogenian warm interval oceans falls in the 1.1-1.5‰ range. Low Mo concentrations (0.9–3.5 ppm) and Mo/TOC (1.5–3.3) in the euxinic part of the Arena Fm compared to modern environments is also a general trend observed in the Datangpo Fm and other pre-Marinoan samples (Scott et al., 2008; Dahl et al., 2010; Cheng et al., *this issue*). This finding implies that low Mo availability in the global ocean environment is a characteristic feature of the Cryogenian. In combination with the estimated ~4 fold lower Mo concentration in Cryogenian seawater compared to modern oceans, our observations indicate a global ocean with extensive euxinia occurring after the Sturtian glaciation.

According to a model for the Mo cycle in the ancient oceans (Dahl et al., 2011), there is no need for an oxygenated deep ocean (today Mn-oxides in the deep ocean accounts for 30–50% of global Mo burial). Model predictions show that euxinic conditions covering 0.1–1.0% of the seafloor would lead to oceanic δ^{98}Mo of 1.1–1.5‰ and 3-6 fold lower Mo concentrations than the modern ocean (Dahl et al., 2011). This is a 2–20 fold greater extent of euxinic seafloor area compared to modern oceans and similar to the Pre-Sturtian ocean state (Dahl et al., 2011). By inference, sulfidic waters masses extended beyond restricted fjords and occurred in continental shelves during the Cryogenian warm interval, which is also exemplified in the Arena, Datangpo and Black River Dolomite basins. Still, anoxic and ferruginous waters were likely even more pervasive on the continental shelves and the deep ocean could well have been anoxic (Canfield et al., 2008; Dahl et al., 2010b; Sperling et al., 2015).

Molybdenum isotopic evidence from euxinic shales in Greenland, China and Australia suggests that euxinic ocean conditions still prevailed after the Sturtian

glaciation. Hence, we find no evidence that the thawing of the Sturtian Snowball led to massive ocean oxygenation (Feng et al., 2010; Li et al., 2012; Zhang et al., 2015; Cheng et al., *this issue*; Kendall et al., 2015). This observation differs from findings in recent studies of U isotopes in the Taishir Fm, Mongolia. These studies show a contrasting development in the global ocean oxygenation state after the Sturtian glaciation (Lau et al., 2017). Mass balance analyses of the $\delta^{238}U$ results showed a period of ocean oxygenation immediately after the Sturtian glaciation followed by a return to anoxia at the onset of the negative Taishir $\delta^{13}C_{CARB}$ excursion (Lau et al., 2017). The marine U cycle is sensitive to sediment burial in anoxic settings, whereas the Mo cycle depends on hydrogen sulphide present in the anoxic waters (Dahl et al., 2014). Therefore, it is hard to reconcile how the marine Mo cycle could be in a more sulfidic anoxic state when the marine U cycle was in an oxygenated state.

We offer two solutions to the problem. First, it is theoretically possible that the Mo and U data do not overlap in time. The positive $\delta^{13}C_{ORG}$ transition in the Arena Fm may indicate that it was deposited only during the anoxic period of the Tayshir excursion, missing the oxygenated period leading up to it. This would require that the Arena Fm, Datangpo and Black River Dolomite only represented the later pervasively anoxic period of the interglacial interval. Higher chrono- and chemostratigraphic resolution of the respective sampling locations can clarify whether these shale formations contain the earlier part of the Cryogenian interglacial. Secondly, the lower Taishir Fm may carry a false oxygenation signature prior to the Taishir $\delta^{13}C$ anomaly; for example by incorporation of reduced U (as indicated by elevated U contents in this part of the two studied sections) (Lau et al., 2016). This behavior is exemplified in some Late Cambrian argillaceous limestones (Dahl et al., 2014). To test this idea, we recommend further uranium isotope studies from coeval limestone sections

elsewhere in the world. These arguments would imply that anoxic ocean conditions were pervasive throughout the Cryogenian warm interval.

5.6 Ocean redox state and animal evolution

According to observations in this study, ocean oxygenation did not follow the termination of the Sturtian glaciation. However, chemostratigraphic constraints are needed to correlate the Arena Fm with the Tayshir Fm and additional U isotope studies are needed to validate the global oxygenation episode recorded in the Taishir Fm (Lau et al., 2016). After the Marinoan glaciation, several studies suggest episodes of widespread ocean oxygenation (Kendall et al., 2015; Sahoo et al., 2012) superimposed on a predominantly anoxic Ediacaran ocean state (Canfield et al. 2008; Sahoo et al., 2016; Sperling et al., 2015). Therefore, we ask what made the post-Marinoan interval different from the post-Sturtian deglaciation?

Marine oxygen levels are determined by the balance between O_2 supply from the atmosphere and O_2 consumption within the oceans. Atmospheric O_2 levels are linked to continental weathering via oceanic nutrient supply, marine primary productivity and organic carbon burial (Lenton et al., 2014). Model predictions suggest global weathering rates increases ~10 fold in the aftermath of a Snowball glaciation (Le Hir et al., 2009). This increase could fertilize the oceans and thereby increase marine O_2 consumption, and at the same time sustain more organic carbon burial that would increase atmospheric pO_2 if sustained over million year time scales (Lenton et al., 2014; Mills et al., 2011; Planavsky et al. 2010). Our data indicate that marine oxygen consumption kept pace with any putative rise in dissolved O_2 levels in the surface ocean resulting from atmospheric oxygenation after the Sturtian glaciation.

Nevertheless, we cannot exclude that ocean oxygenation occurred as a delayed response to increased weathering rates during a subsequent period of time not represented by the Arena Fm .

In contrast, biological driving factors could well reorganize the marine carbon cycle and cause widespread ocean oxygenation. During the Late Neoproterozoic, eukaryotic algae replaced cyanobacteria as the most abundant primary producer and animals with bilaterian, diploblastic, and poriferan body plans appeared (Erwin et al., 2011; Knoll, 2014). The larger organisms might have driven an internal reorganization of the marine carbon cycle necessary to drive ocean oxygenation in at least two ways. For example,

1) Filter-feeding organisms (e.g. sponges, cnidaria) emerging in the Tonian and Cryogenian oceans were capable of clearing the water column of organic material, especially the smallest picoplankton and dissolved organic matter (Peterson et al., 2004; Love et al., 2009; Maloof et al., 2010; Erwin et al., 2011; Sperling et al., 2015 (b)). Thus, sponges might have removed dissolved organic matter from the water column and thereby reduced the oxygen demand in the shallow oceans, and also allowing light to penetrate deeper into the water column giving a selective advantage for larger eukaryotic algae (Butterfield, 2009; Lyons et al., 2014; Lenton et al., 2014). In turn, this process could have removed a large O_2 sink within the oceans and thereby oxygenated the oceans (Butterfield, 2009a, b; Lenton et al., 2014). It might even have generated a positive feedback loop if filter-feeding organisms invaded new areas of the seafloor or became more efficient in increasingly oxygenated oceans (Lenton et al., 2014).

2) The size of zooplankton and their fecal pellets is another a key factor dictating organic carbon export to the sediment-water interface (Logan et al., 1995).

An increase in fecal pellet size would cause an increase in the sinking velocity of organic particles through the water column. Due to greater decomposition depths, the ocean surface became increasingly oxygenated and hydrogen sulfide production was confined to the ocean floor rather than in the water column (Canfield, 2014; Lenton et al., 2014; Logan et al., 1995).

In both cases, atmospheric oxygenation preceded ocean oxygenation. The Sturtian and Marinoan glaciations did not trigger animal evolution via atmospheric oxygenation. Instead, marine oxygen levels must have already been sufficiently high to meet early animal respiratory needs (Mills and Canfield, 2014). Rather, the Cryogenian icehouse could have promoted animal evolution in other ways (e.g., Boyle et al., 2007), so that the delayed biological reorganizations by animals promoted further ocean oxygenation and reinforced the establishment of metazoan ecosystems in the Ediacaran and Cambrian.

6. Conclusion

This study investigated the chemostratigraphy and ocean redox conditions of the Arena Fm, East Greenland. Based on a correlation between $\delta^{13}C$ chemostratigraphy and extremely heavy $\delta^{34}S$, the deposits of the Arena Fm represent the warm interval between the Sturtian and Marinoan glaciations. The $\delta^{13}C_{CARB}$ record has been diagenetically altered by $\delta^{13}C$-depleted meteoric water and dolomitizing fluids. Iron-based proxies show that the depositional environment was anoxic, and transitioned from euxinic conditions near the base of the succession to ferruginous conditions up-section. Very low Mo concentrations and a Mo–TOC correlation with a shallow slope in the euxinic interval suggest that the Arena basin was hydrographically restricted and that dissolved Mo was ~4-fold lower in Cryogenian seawater compared to the

present day. The maximum δ^{98}Mo value recorded in the euxinic Arena shales is 1.5‰, which is well below that of the modern oceans (2.3‰). A decreasing trend of δ^{98}Mo upsection is correlated with an inferred decline in the concentration of bottom water H_2S in the basin, culminating in strongly fractionated δ^{98}Mo values (-0.86‰). These very low values are likely due to the removal of Mo from the water column in association with Fe-oxide minerals, and/or incomplete thiomolybdate conversion at low H_2S availability (< 11 µM). In combination with the highest δ^{98}Mo values observed in contemporary euxinic basins (Datangpo Fm, China, and Black River Dolomites, Tasmania), our results indicate that the deep oceans were not fully oxygenated and that a ~0.1–1% fraction of the global seafloor remained pervasively euxinic in the aftermath of the Sturtian glaciation. Therefore, we infer that if enhanced weathering occurred, it did not significantly perturb the extent of euxinia in the oceans. These observations contrast with global redox studies in carbonates of the Taishir Fm, Mongolia. Further global ocean redox constraints and better chemostratigraphic resolution are necessary to settle discrepancies in interpretation of the redox conditions in the Cryogenian warm interval and the link between Snowball glaciations and ocean oxygenation.

7. Appendices

Table 1: Supplementary data table

Acknowledgements

Thanks H. Grøn Jensen and B. Petersen for laboratory assistance. KKK thanks the organizers and field assistance of Bjørn Buchardt and Svend Stouge during fieldwork in August 2005. TWD acknowledges Minik Rosing for field assistance during field

work in 2011 and Christian Bjerrum for use of handheld X-Ray Fluorescence analyzer. This project was funded by the Villum Foundation to TWD (1168439, VKR023127). Field trip to East Greenland in 2007 was funded by the Carlsberg Foundation, and the 2011 field campaign with expedition ship, S/V Activ led by Captain Jonas Bergsøe was funded by Skibsreder Carsten Brebøls Almenyttige Fond and Dr. Frederik Paulsen. We thank the Carlsberg Foundation Distinguished Associate Professor Fellowship (TWD), Independent Research Fund Denmark (TWD, CK) and the Villum Foundation (DEC) for financial support.

References

Ahm, A.C., Bjerrum, C.J., Hammarlund, E.U., 2017. Disentangling the record of diagenesis, local redox conditions, and global seawater chemistry during the latest Ordovician glaciation. Earth and Planetary Science Letters 459, 145-156.

Aller, R.C., Mackin, J.E., Cox, R.T., 1986. Diagenesis of Fe and Si in Amazon Inner Shelf Muds - Apparent Dominance of Fe Reduction and Impliations for the Genesis of Ironstones. Cont. Shelf Res. 6, 263-289.

Anderson, T.F., Raiswell, R., 2004. Sources and mechanisms for the enrichment of highly reactive iron in euxinic Black Sea sediments. American Journal of Science 304, 203-233.

Archer, C., Vance, D., (2008). The isotopic signature of the global riverine molybdenum fux and anoxia in the ancient oceans. Nat Geosci 1, 597–600.

Arnold, G.L., Anbar, A.D., Barling, J., Lyons, T.W., 2004. Molybdenum isotope evidence for widespread anoxia in mid-proterozoic oceans. Science 304, 87–90.
Aller, R.C., Mackin, J.E., Cox, R.T., 1986. Diagenesis of Fe and Si in Amazon Inner Shelf Muds - Apparent Dominance of Fe Reduction and Impliations for the Genesis of Ironstones. Cont. Shelf Res. 6, 263-289.

Archer, C., Vance, D., 2008. The isotopic signature of the global riverine molybdenum flux and anoxia in the ancient oceans. Nature Geoscience 1, 597-600.

Arnold, G.L., Anbar, A.D., Barling, J., Lyons, T.W., 2004. Molybdenum isotope evidence for widespread anoxia in mid-proterozoic oceans. Science 304, 87–90.

Baldwin, G.J., Nägler, T.F., Greber, N.D., Turner, E.C., Kamber, B.S., 2013. Mo isotopic composition of the mid-Neoproterozoic ocean: An iron formation perspective. Precambrian Research 230, 168-178.

Bold, U., Smith, E.F., Rooney, A.D., Bowring, S.A., Buchwaldt, R., Dudás, F.Ő., Ramezani, J., Crowley, J.L., Schrag, D.P., Macdonald, F.A., 2016. Neoproterozoic stratigraphy of the Zavkhan terrane of Mongolia: The backbone for Cryogenian and early Ediacaran chemostratigraphic records. Am. J. Sci. 316, 1-63.

Boyle, R.A., Lenton, T.M., Williams, H.T.P., 2007. Neoproterozoic 'snowball Earth' glaciations and the evolution of altruism. Geobiology 5, 337-349.

Butterfield, N.J., 2009a. Macroevolutionary turnover through the Ediacaran transition: ecological and biogeochemical implications. Geological Society, London, Special Publications 326, 55-66.

Butterfield, N.J., 2009b. Oxygen, animals and oceanic ventilation: an alternative view. Geobiology 7, 1-7.

Canfield, D., Raiswell, R., Westrich, J.T., Reaves, C.M., Berner, R.A., 1986. The Use of Chromium Reduction in the Analysis of Reduced Inorganic Sulfur in Sediments and Shales. Chemical Geology 54, 149-155.

Canfield, D.E., 2004. The Evolution of Earth Surface Sulfur Reservoir. Am J Sci 304, 839–861.

Canfield, D.E., 2014. Oxygen: a four billion year history. Princeton University Press.

Canfield, D.E., Poulton, S.W., Knoll, A.H., Narbonne, G.M., Ross, G., Goldberg, T., Strauss, H., 2008. Ferruginous conditions dominated later neoproterozoic deep-water chemistry. Science 321, 949-952.

Clarkson, M.O., Poulton, S.W., Guilbaud, R., Wood, R.A., 2014. Assessing the utility of Fe/Al and Fe-speciation to record water column redox conditions in carbonate-rich sediments. Chemical Geology 382, 111-122.

Dahl, T.W., Anbar, A.D., Gordon, G.W., Rosing, M.T., Frei, R., Canfield, D.E., 2010a. The behavior of molybdenum and its isotopes across the chemocline and in the sediments of sulfidic Lake Cadagno, Switzerland. Geochimica et Cosmochimica Acta 74, 144–163.

Dahl, T.W., Boyle, R.A., Canfield, D.E., Connelly, J.N., Gill, B.C., Lenton, T.M., Bizzarro, M., 2014. Uranium isotopes distinguish two geochemically distinct stages during the later Cambrian SPICE event. Earth and Planetary Science Letters 401, 313-326.

Dahl, T.W., Canfield, D.E., Rosing, M.T., Frei, R.E., Gordon, G.W., Knoll, A.H., Anbar, A.D., 2011. Molybdenum evidence for expansive sulfidic water masses in ~750Ma oceans. Earth and Planetary Science Letters 311, 264-274.

Dahl, T.W., Hammarlund, E.U., Anbar, A.D., Bond, D.P.G., Gill, B.C., Gordon, G.W., Knoll, A.H., Nielsen, A.T., Schovsbo, N.H., Canfield, D.E., 2010b. Devonian

rise in atmospheric oxygen correlated to the radiations of terrestrial plants and large predatory fish. Proceedings of the National Academy of Sciences 107, 17911–17915.

Dahl, T.W., Ruhl, M., Hammarlund, E.U., Canfield, D.E., Rosing, M.T., Bjerrum, C.J., 2013. Tracing euxinia by molybdenum concentrations in sediments using handheld x-ray fluorescence spectroscopy (HH-XRF). Chemical Geology 360–361, 241–251.

Dahl, T.W., Wirth, S.B., 2017. Molybdenum isotope fractionation and speciation in a euxinic lake - testing ways to discern isotope fractionation processes in a sulfidic setting. Chemical Geology 460, 84–92.

Dickson, A.J., Jenkyns, H.C., Porcelli, D., van den Boorn, S., Idiz, E., 2016. Basin-scale controls on the molybdenum-isotope composition of seawater during Oceanic Anoxic Event 2 (Late Cretaceous). Geochimica et Cosmochimica Acta 178, 291-306.

Einsele, G., 2013. Sedimentary basins: evolution, facies, and sediment budget. Springer Science & Business Media.

Erwin, D.H., Laflamme, M., Tweedt, S.M., Sperling, E.A., Pisani, D., Peterson, K.J., 2011. The Cambrian conundrum: early divergence and later ecological success in the early history of animals. Science 334, 1091-1097.

Fairchild, I.J., Hambrey, M.J., 1995. Vendian Basin Evolution in East Greenland and NE Svalbard. Precambrian Res. 73, 217-233.

Feng, L.-J., Chu, X.-L., Huang, J., Zhang, Q.-R., Chang, H.-J., 2010. Reconstruction of paleo-redox conditions and early sulfur cycling during deposition of the Cryogenian Datangpo Formation in South China. Gondwana Research 18, 632-637.

Goldberg, T., Archer, C., Vance, D., Poulton, S.W., 2009. Mo isotope fractionation during adsorption to Fe (oxyhydr)oxides. Geochimica et Cosmochimica Acta 73, 6502-6516.

Halevy, I., Peters, S.E., Fischer, W.W., 2012. Sulfate Burial Constraints on the Phanerozoic Sulfur Cycle. Science 337, 331–334.

Halverson, G., Shields-Zhou, G., 2011. Chemostratigraphy and the Neoproterozoic glaciations, in: Arnaud, E., Halverson, G., Shields-Zhou, G. (Eds.), The Geological Record of Neoproterozoic Glaciations. Geological Society, London, pp. 51–66.

Halverson, G.P., Maloof, A.C., Hoffman, P.F., 2004. The Marinoan glaciation (Neoproterozoic) in northeast Svalbard. Basin Research 16, 297-324.

Halverson, G.P., Wade, B.P., Hurtgen, M.T., Barovich, K.M., 2010. Neoproterozoic chemostratigraphy. Precambrian Research 182, 337-350.

Hambrey, M.J., Spencer, A.M., 1987. Late Precambrian glaciation of central east Greenland. Nyt Nordisk Forlag.

Hoffman, P.F., Halverson, G.P., Domack, E.W., Maloof, A.C., Swanson-Hysell, N.L., Cox, G.M., 2012. Cryogenian glaciations on the southern tropical paleomargin of

Laurentia (NE Svalbard and East Greenland), and a primary origin for the upper Russøya (Islay) carbon isotope excursion. Precambrian Research 206-207, 137-158.

Kendall, B., Creaser, R.A., Selby, D., 2006. Re-Os geochronology of postglacial black shales in Australia: Constraints on the timing of "Sturtian" glaciation. Geology 34, 729.

Kendall, B., Dahl, T.W., Anbar, A.D., 2017. The Stable Isotope Geochemistry of Molybdenum. Reviews in Mineralogy and Geochemistry 82, 683–732.

Kendall, B., Komiya, T., Lyons, T.W., Bates, S.M., Gordon, G.W., Romaniello, S.J., Jiang, G., Creaser, R.A., Xiao, S., McFadden, K., Sawaki, Y., Tahata, M., Shu, D., Han, J., Li, Y., Chu, X., Anbar, A.D., 2015. Uranium and molybdenum isotope evidence for an episode of widespread ocean oxygenation during the late Ediacaran Period. Geochimica et Cosmochimica Acta 156, 173-193.

Kilner, B., Mac Niocaill, C., Stouge, S., Harper, D., 2004. Palaeomagnetism of the Late Neoproterozoic of Ella O, North-East Greenland, AGU Fall Meeting Abstracts.

Knoll, A.H., 2014. Paleobiological perspectives on early eukaryotic evolution. Cold Spring Harb Perspect Biol 6.

Knoll, A.H., Hayes, J.M., Kaufman, A.J., Swett, K., Lambert, I.B., 1986. Secular variation in carbon isotope ratios from Upper Proterozoic successions of Svalbard and East Greenland. Nature.

Knoll, A.H., Swett, K., 1987. Micropaleontology across the Precambrian-Cambrian Boundary in Spitsbergen. J. Paleontol. 61, 898–926.

Kristiansen, K., 2007. En undersøgelse af de palæoklimatiske forhold (Snowball Earth) i Tillit Gruppen og tilgrænsende aflejringer, Eleonore Bay Supergruppe, Nordøstgrønland, baseret på isotopgeokemiske metoder, Geological Institute. University of Copenhagen, Copenhagen, p. 95.

Kunzmann, M., Halverson, G.P., Scott, C., Minarik, W.G., Wing, B.A., 2015. Geochemistry of Neoproterozoic black shales from Svalbard: Implications for oceanic redox conditions spanning Cryogenian glaciations. Chemical Geology 417, 383-393.

Lau, K.V., Macdonald, F.A., Maher, K., Payne, J.L., 2016. Uranium isotope evidence for temporary ocean oxygenation in the aftermath of the Sturtian Snowball Earth. Earth and Planetary Science Letters 458, 282–292.

Le Hir, G., Donnadieu, Y., Goddéris, Y., Pierrehumbert, R.T., Halverson, G.P., Macouin, M., Nédélec, A., Ramstein, G., 2009. The snowball Earth aftermath: Exploring the limits of continental weathering processes. Earth and Planetary Science Letters 277, 453-463.

Lenton, T.M., Boyle, R.A., Poulton, S.W., Shields-Zhou, G.A., Butterfield, N.J., 2014. Co-evolution of eukaryotes and ocean oxygenation in the Neoproterozoic era. Nature Geosci 7, 257–265.

Li, C., Love, G.D., Lyons, T.W., Scott, C.T., Feng, L., Huang, J., Chang, H., Zhang, Q., Chu, X., 2012. Evidence for a redox stratified Cryogenian marine basin, Datangpo Formation, South China. Earth and Planetary Science Letters 331-332, 246-256.

Li, Z.X., Bogdanova, S.V., Collins, A.S., Davidson, A., De Waele, B., Ernst, R.E., Fitzsimons, I.C.W., Fuck, R.A., Gladkochub, D.P., Jacobs, J., Karlstrom, K.E., Lu, S., Natapov, L.M., Pease, V., Pisarevsky, S.A., Thrane, K., Vernikovsky, V., 2008. Assembly, configuration, and break-up history of Rodinia: A synthesis. Precambrian Research 160, 179-210.

Logan, G.A., Hayes, J.M., Hieshima, G.B., Summons, R.E., 1995. Terminal Proterozoic reorganization of biogeochemical cycles. Nature 376, 53–56.

Lyons, T.W., Severmann, S., 2006. A critical look at iron paleoredox proxies: New insights from modern euxinic marine basins. Geochimica et Cosmochimica Acta 70, 5698-5722.

Mac Niocaill, C., Kilner, B., Stouge, S., Harper, D., Knudsen, M., Christiansen, J., 2008. The Neoproterozoic drift history of Laurentia: a critical evaluation and new palaeomagnetic data from Northern and Eastern Greenland, AGU Spring Meeting Abstracts.

Mac Niocaill, C., Stouge, S., Harper, D., Christiansen, J., Kilner, B., Johnson, A., Watts, C., 2004. Preliminary paleomagnetic results from the late Neoproterozoic of eastern Greenland: A low-latitude Sturtian glaciation?, AGU Spring Meeting Abstracts.

Martin, J.-M., Meybeck, M., 1979. Elemental mass-balance of material carried by major world rivers. Mar. Chem. 7, 173-206.

Miller, C.A., Peucker-Ehrenbrink, B., Walker, B.D., Marcantonio, F., 2011. Re-assessing the surface cycling of molybdenum and rhenium. Geochimica et Cosmochimica Acta 75, 7146-7179.

Moczydlowska, M., Pease, V., Willman, S., Wickström, L., Agic, H., 2017. A Tonian age for the Visingsö Group in Sweden constrained by detrital zircon dating and biochronology: implications for evolutionary events. Geol. Mag., 1-15.

Neubert, N., Nägler, T.F., Böttcher, M.E., 2008. Sulfidity controls molybdenum isotope fractionation into euxinic sediments: Evidence from the modern Black Sea. Geology 36, 775–778.

Pearce, C.R., Cohen, A.S., Parkinson, I.J., 2009. Quantitative Separation of Molybdenum and Rhenium from Geological Materials for Isotopic Determination by MC-ICP-MS. Geostandards and Geoanalytical Research 33, 219–229.

Poulton, S., Canfield, D., 2005. Development of a sequential extraction procedure for iron: implications for iron partitioning in continentally derived particulates. Chemical Geology 214, 209–221.

Raiswell, R., Berner, R.A., 1985a. Pyrite and Organic-Matter in Phanerozoic Normal Marine Shales. Geochimica et Cosmochimica Acta 50, 1967–1976.

Raiswell, R., Berner, R.A., 1985b. Pyrite Formation in Euxinic and Semi-Euxinic Sediments. Am J Sci 285, 710–724.

Ries, J.B., Fike, D.A., Pratt, L.M., Lyons, T.W., Grotzinger, J.P., 2009. Superheavy pyrite (34Spyr > 34SCAS) in the terminal Proterozoic Nama Group, southern Namibia: A consequence of low seawater sulfate at the dawn of animal life. Geology 37, 743-746.

Rooney, A.D., Macdonald, F.A., Strauss, J.V., Dudas, F.O., Hallmann, C., Selby, D., 2014. Re-Os geochronology and coupled Os-Sr isotope constraints on the Sturtian snowball Earth. Proc Natl Acad Sci U S A 111, 51-56.

Sahoo, S.K., Planavsky, N.J., Kendall, B., Wang, X., Shi, X., Scott, C., Anbar, A.D., Lyons, T.W., Jiang, G., 2012. Ocean oxygenation in the wake of the Marinoan glaciation. Nature 489, 546-549.

Sarmiento, J.L., Gruber, N., 2006. Ocean Biogeochemical Dynamics. Princeton university press, New Jersey, USA.

Scott, C., Lyons, T.W., 2012. Contrasting molybdenum cycling and isotopic properties in euxinic versus non-euxinic sediments and sedimentary rocks: Refining the paleoproxies. Chemical Geology 324-325, 19-27.

Scott, C., Lyons, T.W., Bekker, A., Shen, Y., Poulton, S.W., Chu, X., Anbar, A.D., 2008. Tracing the stepwise oxygenation of the Proterozoic ocean. Nature 452, 456-459.

Sperling, E.A., Wolock, C.J., Morgan, A.S., Gill, B.C., Kunzmann, M., Halverson, G.P., Macdonald, F.A., Knoll, A.H., Johnston, D.T., 2015. Statistical analysis of iron geochemical data suggests limited late Proterozoic oxygenation. Nature 523, 451-454.

Taylor, S.R., McLennan, S.M., 1995. The geochemical evolution of the continental crust. Rev. Geophys. 33, 241–265.

Ullmann, C.V., Campbell, H.J., Frei, R., Hesselbo, S.P., Pogge von Strandmann, P.A.E., Korte, C., 2013. Partial diagenetic overprint of Late Jurassic belemnites from New Zealand: Implications for the preservation potential of δ7Li values in calcite fossils. Geochimica et Cosmochimica Acta 120, 80-96.

Vidal, G., 1976. Late Precambrian acritarchs from the Eleonora Supergroup and Tillite Group in East Greenland. The Geological Survey of Greenland, Copenhagen.

Vidal, G., 1979. Acritarchs from the Upper Proterozoic and Lower Cambrian of East Greenland. Bull. Grønlands Geol. Unders. 134, 7 pls.

Vidal, G., 1981. Aspects of problematic acid-resistant, organic-walled microfossils (acritarchs) in the upper Proterozoic of the north atlantic region. Precambrian Res. 15, 9–23.

Zhabina, N.N., Volkov, I.I., 1978. A Method of Determination of Various Sulfur Compounds in Sea Sediments and Rocks. Ann Arbor Science Publishers, Mich.

Fig. 1

(A) Map of Greenland and the location of the sampling site, Ella Ø, marked with a red star. (B) Geological map of the Kong Oscar Fjord region indicating the position of Ella Ø (Ella Island). Ella Ø is part of the basin with Neoproterozoic-Ordovician deposits. The Caledonian orogeny caused subsequent tectonic disruptions. (C) Geological map of the field location near Bastionsbugt displaying Bed group 18 (brown), Bed group 19 (red), Ulvesø Fm (yellow), Arena Fm (grey), Storeelv Fm (green), Canyon and Spiral Creak Fm (purple), and Cambrian-Ordovician deposits. (D) Photo of field location at Ella Ø. Spiral Creek Fm (SC) and Ulvesø Fm (UL) can be observed directly on the photo. Modified from Kristiansen (2007).

Fig. 2

Lithological and chemostratigraphic data from the Arena Fm. The Arena Fm mainly consists of shales with three layers of sandstone. $\delta^{13}C_{CARB}$ (squares), $\delta^{18}O_{CARB}$ (triangles), $\delta^{13}C_{ORG}$ (diamonds) and $\delta^{34}S$ (circles) comprise the chemostratigraphic data discussed in this paper. Ages of Sturtian and Marinoan glaciations are summarized in Bold et al., 2016 and Rooney et al., 2014.

Fig. 3

Geochemical data from the Arena Fm in stratigraphic context. Abbreviations: TOC – Total Organic Carbon (white triangles), ratio of highly reactive to total iron – Fe_{HR}/Fe_T (white squares), ratio of pyrite to highly reactive iron – Fe_P/Fe_{HR} (white diamonds), iron/aluminum ratio – Fe/Al (black triangles), molybdenum concentrations – Mo (white circles), and molybdenum isotope compositions – $\delta^{98}Mo$ (black circles). Three samples with Fe/Al>2 are omitted in the Fe/Al diagram as they

have high carbonaceous content have Fe/Al>2 and their lithological origin is considerably different from typical shales. Deposition under anoxic bottom waters is indicated with grey zones, where Fe/Al > 0.5 and Fe_{HR}/Fe_T > 0.38, although Fe_{HR}/Fe_T > 0.22 is likely also representative of anoxic deposition (Canfield & Raiswell, 2012; Raiswell and Canfield, 2011). Deposition is indicated for anoxic samples with Fe_P/Fe_{HR} > 0.7 (Anderson and Raiswell, 2004; März et al., 2008). Proterozoic average Mo content is 21 ppm (Scott et al., 2008). The average δ^{98}Mo of modern day oceanic input is 0.7‰ (Archer and Vance, 2008). Error bars represent 2 SD (2 standard deviations). Ages of Sturtian and Marinoan glaciations from Bold et al., 2016; Macdonald et al., 2010; Rooney et al., 2014; 2015).

Fig. 4

Bulk rock δ^{98}Mo versus 1/Mo is shown for samples in the Arena Fm. Black circles represent the euxinic samples in the lower Arena Fm, whereas white circles represent ferruginous shales in the upper Arena Fm . The dashed lines indicate δ^{98}Mo isotope compositions of average riverine input (0.7‰) and average crust (0.3‰) (Archer and Vance, 2008)(Kendall et al., 2017). The grey interval indicates the δ^{98}Mo range of crustal igneous rocks (–0.1 to 0.5‰) (Kendall et al., 2017). Most samples have δ^{98}Mo compositions below the range of crustal igneous rock compositions. Additionally, mixing detrital and authigenic Mo with distinct compositions would show linear co-variation in this plot; hence no binary mixing trend is apparent from the data.

Fig. 5

Diagram of δ^{13}C and δ^{18}O isotope compositions of inorganic carbonate in selected samples of the Arena Fm. Note the extreme values of isotope compositions and the

covariance trend. These indicate that secondary processes decreased both $\delta^{13}C$ and $\delta^{18}O$ isotope compositions. Samples denoted by crosses contain high carbonate contents and heavier $\delta^{13}C$ and $\delta^{18}O$ isotope compositions. These four samples are less sensitive to secondary alteration processes and best resemble $\delta^{13}C$ and $\delta^{18}O$ of the penecontemporaneous oceans.

Fig. 6

The iron speciation data depicts the marine redox conditions in the local depositional environment (Poulton & Canfield, 2011). The ratio of highly reactive to total iron (Fe_{HR}/Fe_T) is plotted against the ratio of pyrite to highly reactive iron. The lower part of the Arena Fm (black circles) was deposited under euxinic conditions; see Fig. 3 caption for details. Five samples (crosses) in the lower Arena Fm contain high carbonate contents and high Fe-carbonate enrichments that dilute the euxinic signal, although they precipitated during dominantly euxinic conditions. The upper part of the Arena Fm consists of samples (white circles) deposited in either oxic or anoxic, ferruginous conditions. Fe/Al data suggest the latter (Fig. 3).

Fig. 7

Sedimentary Mo contents versus TOC for samples deposited under euxinic conditions (black) and ferruginous conditions (white). The Fe-carbonate enriched euxinic samples are shown with crosses. The dashed line represents a linear fit between TOC and Mo for the euxinic samples (black circles) with a slope of 1.3±0.3 ppm/wt% (R^2=0.80) indicative of a more restricted basin than the euxinic Datangpo Fm (1.5–19.7 ppm/wt%) and similar to euxinic sediments from the Black River Dolomite, Tasmania (2.2–5.1 ppm/wt%) (Kendall et al., 2015; Cheng et al., this issue).

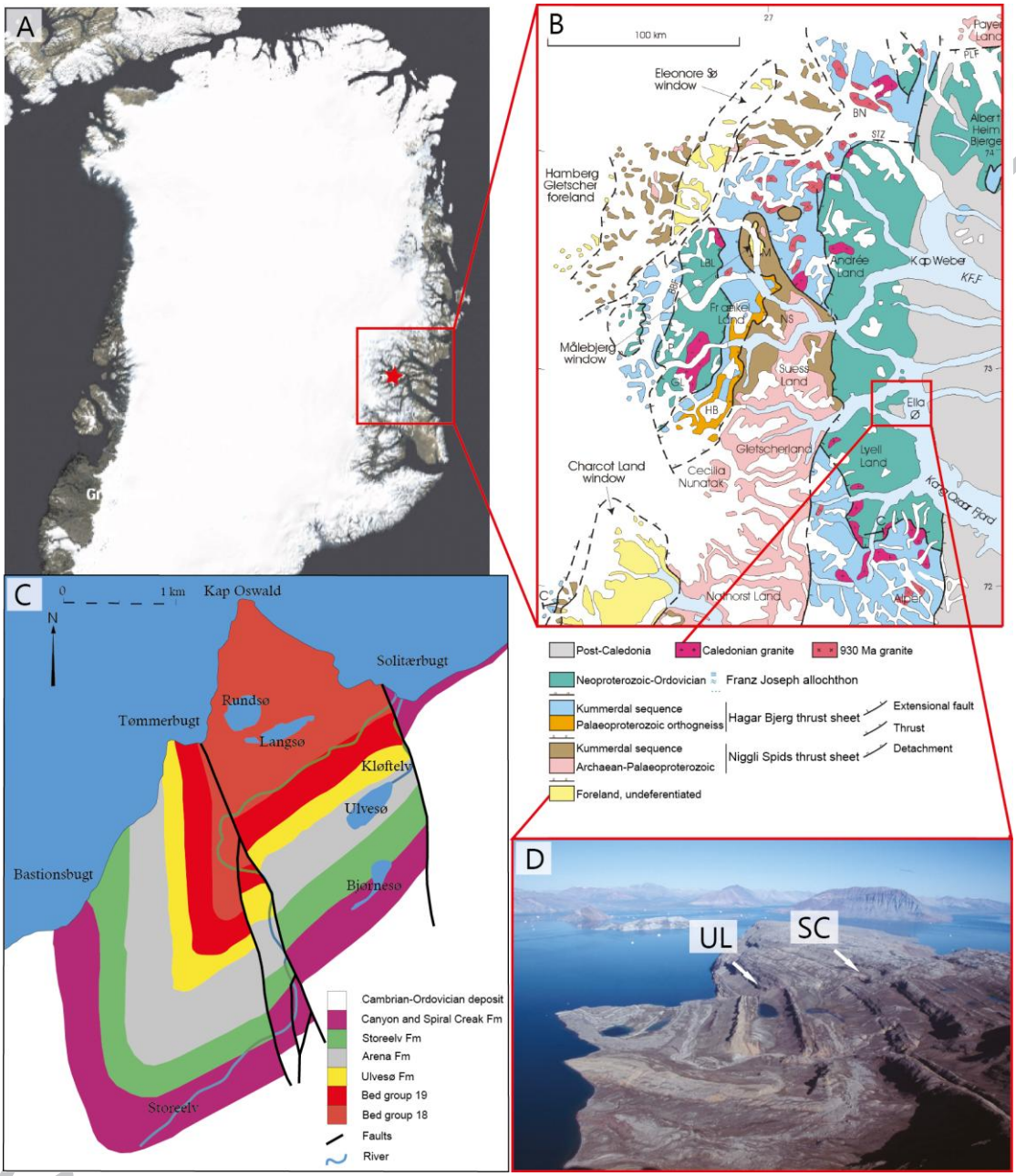

Figure 1

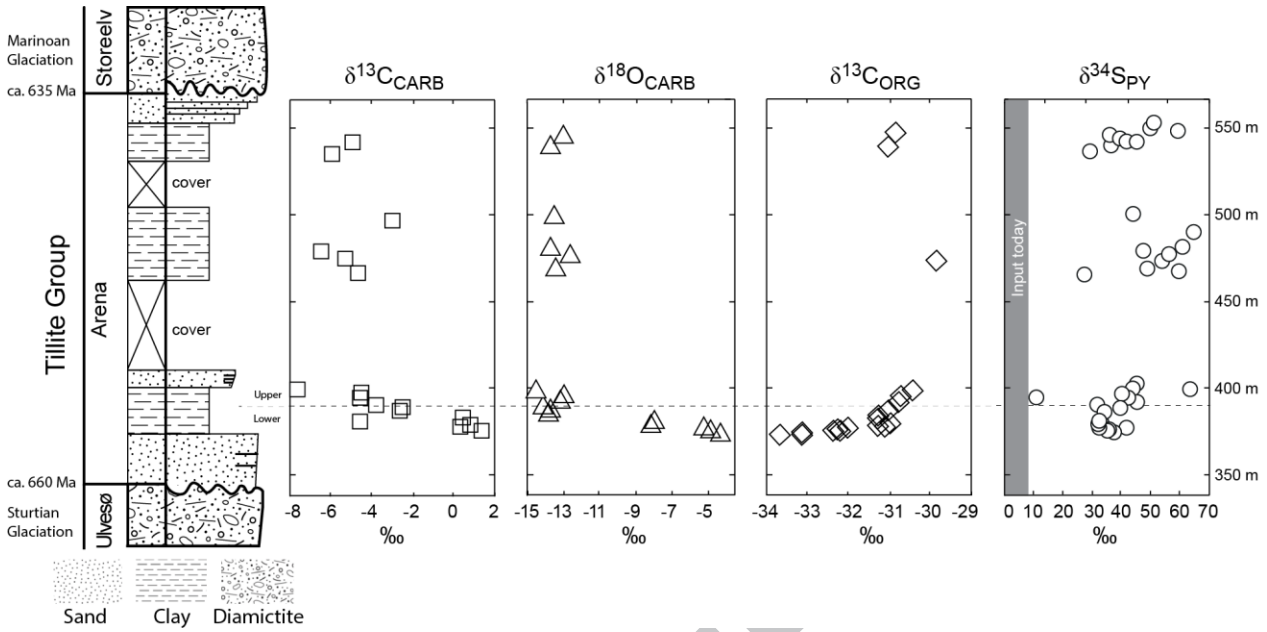

Figure 2

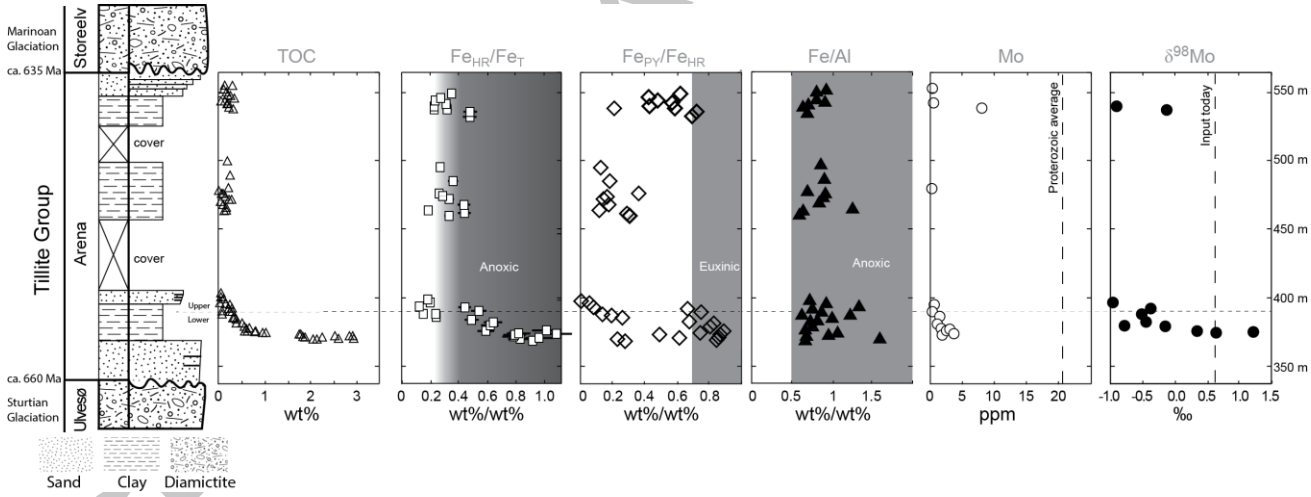

Figure 3

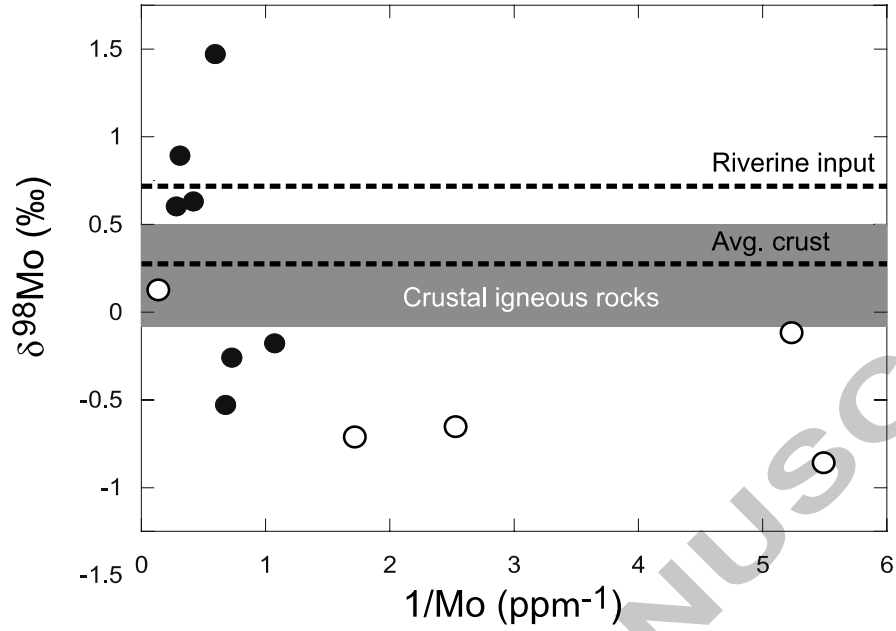

Figure 4

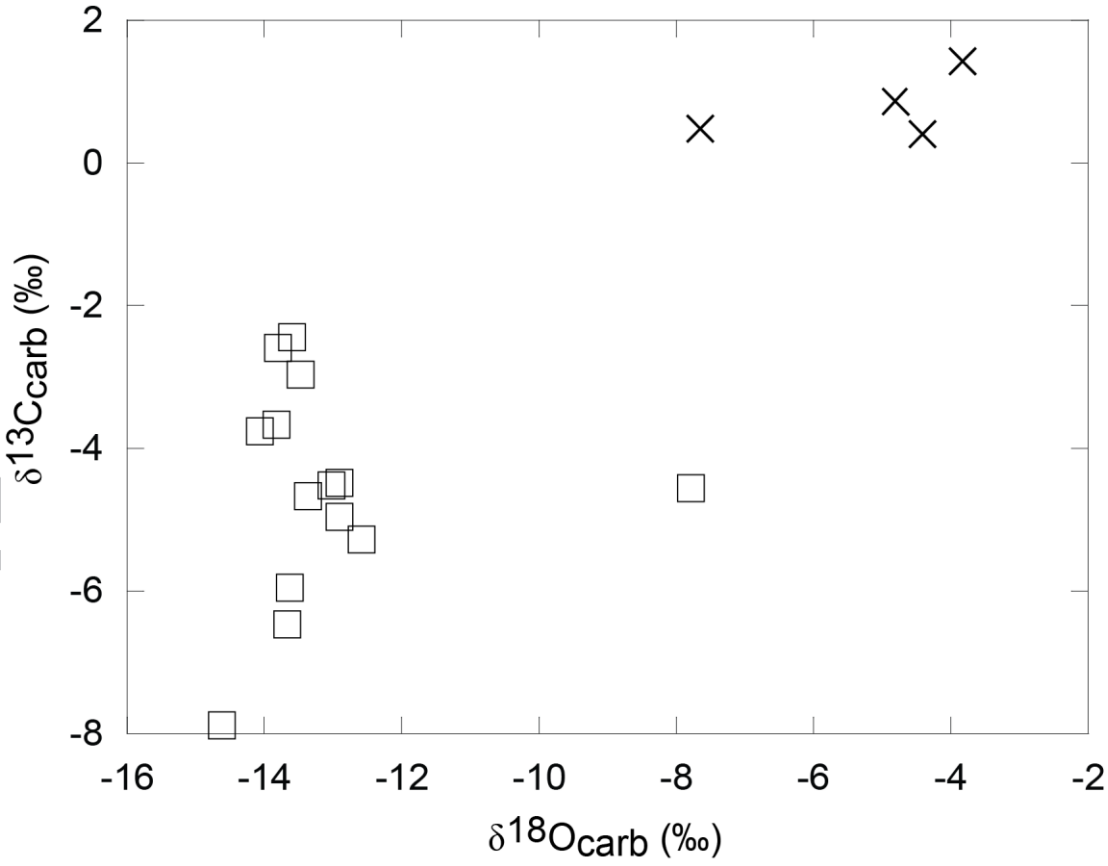

Figure 5

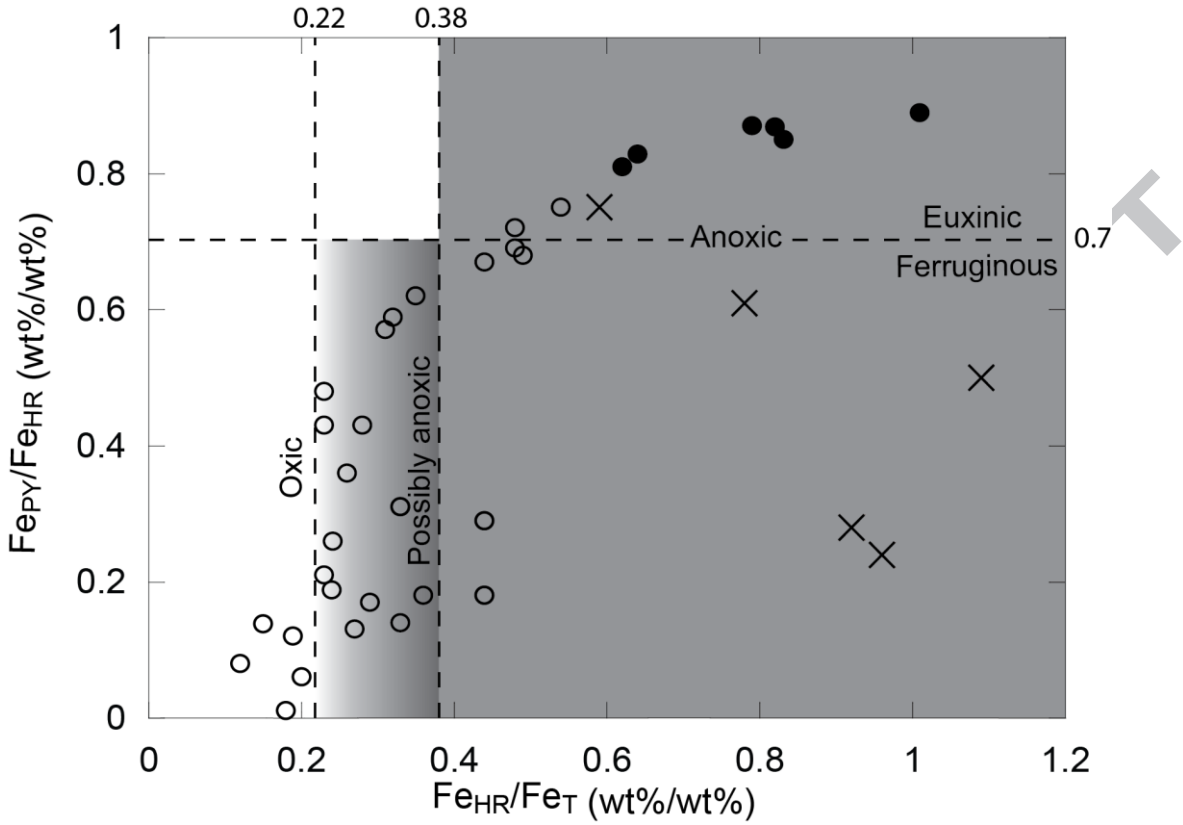

Figure 6

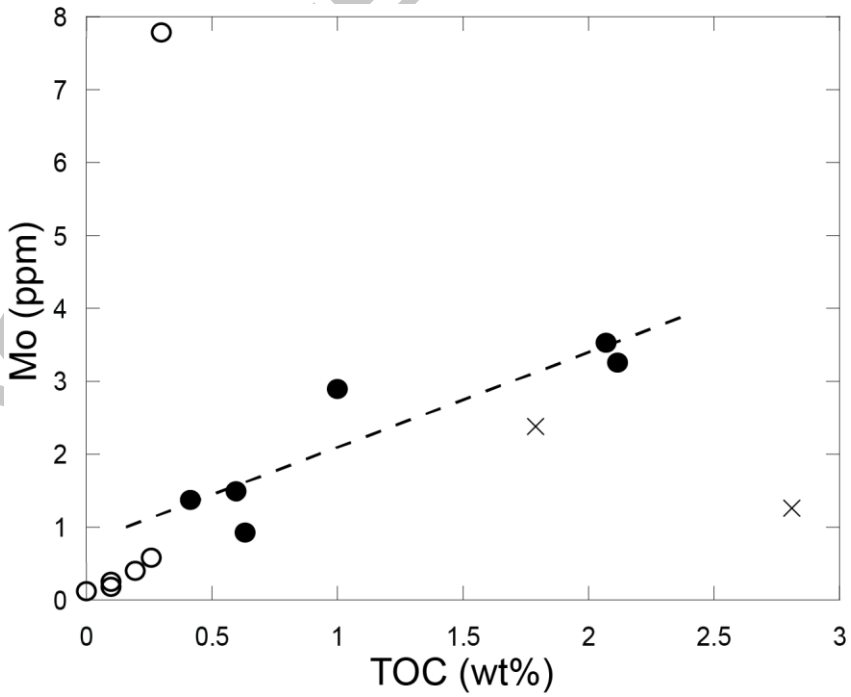

Figure 7

Sample_ID	Stratigraphic_height (m)	δ13CCARB (‰)	δ18OCARB (‰)	δ13CORG (‰)	TC (wt %)	TOC_2006 (wt %)	TOC_2017_replica (wt %)	TS_2006 (wt %)	TS_2017_replica (wt %)	C/S (wt %/wt %)	δ34S (wt %)	δ98Mo (‰)	δ98Mo_auth (‰)	Mo (ppm)	Fet (wt %)	FeCARB (wt %)	FeMAG (wt %)	FeOX (wt %)	FePY (wt %)	FeHR (wt %)	Al (wt %)	1SD Al (wt %)	Fe/Al (wt %/wt %)	Ca (wt %)	1sd Ca (wt %)
K3-22	374.6			-33.7	1.19	2.22	2.21	0.03	1.03	3.2	37.16	0.89	1.02	3.2	5.7*						7.70	0.02	2.23	1.1	1.8
K3_23	375	1.42	-3.83	-33.1		3.0	2.6	0.5	2.7	1.7	34.57	1.47	1.57	1.3	3.5	2.39	-0.09	0.02	0.9	0.32	1.51	0.11	2.3	1.8	1.9
K3_24	376			-33.2	2.20	2.23	1.9	2.4	2.8	0.8	35.60	0.60	0.70	3.5	5.5	0.5	0.02	0.01	3.8	4.5	8.80	0.02	0.7	1.1	1.8
K3_25	376.8	0.40	-4.41	-32.4		2.9	2.6	0.0	2.7	1.9	41.62				4.0	2.9	-0.11	0.01	0.9	3.9	1.99	0.11	2.1	1.8	1.9
K3_26	376.8			-32.2	10.5	3.0		0.0		11.7															
K3	3	0	-	-		1	1	0	3.	1	32		0	2	4	1	0	0	2	3	2	0	1	1	1

3_227	77.8	.86	4.80	32.2		.8	.8	.1	4	.0	.06		.02	.4	.6	.4	.0	.0	.2	.6	.9	.1	.6	2	.9
K3_228	379			-32.0	1.0	1.0	1.0	2.0	2.8	0.4	31.52	0.11	0.18	2.9	5.6	0.4	0.1	0.0	3.8	4.4	8.0	0.2	0.7	1	1.8
K3_229	379.9	-4.56	-7.78	-31.1	9.4	0.8	0.8	0.3	2.7	0.5	32.72	-0.53	-0.53	1.5	2.3	1.4	-0.1	0.0	1.3	2.6	2.4	0.1	1.0	21	1.9
K3_230	380			-31.3	1.5	0.6	0.6	1.9	2.9	0.3	32.49				5.6	0.4	0.1	0.0	4.0	4.6	8.3	0.2	0.7	1	1.8
K3_231	381.8	0.48	-7.65	-31.0	4.1	0.6	0.6	0.7	2.5	0.4	32.34				5.0	0.7	0.1	0.0	2.2	3.0	4.7	0.2	1.1	9	1.9
K3_232	382.4			-31.2	1.0	0.6	0.7	1.6	2.9	0.3		-0.18	-0.02	0.9	6.0	0.4	0.2	0.1	5.4	6.1	8.9	0.2	0.7	1	1.8
K3_233	384			-31.3	1.0	0.5		1.6		0.3															
K3_234	386	-2.59	-13.80	-31.3	0.6	0.5	0.4	1.2	2.5	0.2	34.16				6.3	0.4	0.3	0.1	3.1	3.9	8.1	0.2	0.8	2	1.8
K3_2	388.2	-2.4	-13.	-31.	1.0	0.5	0.4	1.6	2.4	0.2	39.45	-0.2	-0.2	1.4	6.1	0.3	0.3	0.0	3.2	3.9	8.2	0.2	0.7	2	1.8

35		5	58	0								6	0												
K3_236	390	-3.77	-14.06		0.7	0.3	0.3	0.8	1.7	0.3	31.76				6.4	0.5	0.5	0.0	2.1	3.1	7.7	0.2	0.8	2	1.8
K3_237	392.2				1.7	0.1		0.2		0.5	45.19	-0.12	-1.3	0.2	6.6	0.5	0.7	0.1	0.4	1.6	6.6	0.2	1.0	5	1.8
K3_238	394.15	-4.53	-13.02	-30.8	0.9	0.3	0.3	0.4	0.2	1.0	10.82				5.5	0.3	0.6	0.2	0.3	1.3	8.6	0.2	0.6	2	1.8
K3_239	394.4				0.3	0.1		0.1		0.7	41.90				9.4	0.5	0.6	0.1	0.2	1.4	7.7	0.2	1.2	2	1.8
K3_240	396.4	-4.49	-12.91	-30.7	1.1	0.2	0.3	1.3	2.3	0.1	40.05	-0.71	-1.0	0.6	6.9	0.4	0.5	0.1	2.8	3.8	7.8	0.2	0.9	2	1.8
K3_241	399			-30.4	0.3	0.2		0.9		0.3	63.40				6.3	0.4	0.5	0.1	1.9	2.8	8.3	0.2	0.8	1	1.8
K3_242	399.7	-7.88	-14.62		0.8	0.0	0.1	0.0	0.0	4.0	44.10				6.1	0.3	0.4	0.0	0.1	0.7	4.6	0.2	1.3	8	1.9
K3_243	402.5				0.2	0.1		0.0		2.5	45.17				8.8	0.5	0.9	0.2	0.1	1.7	9.4	0.2	0.9	1	1.8
K4	4				0	0	0	0	0.	1	<				6	0	0	0	0	1	9	0	0	1	1

3_2444	04.5				.1	.0	.1	.0	0	0.6	DL	.6	.4	.7	.1	.0	.2	.0	.2	.7		.8
K3_2445	406.5				0.0	0.0		0.0		4.4												
K3_2448	465				0.2	0.1	0.2	0.3	0.5	0.3	26.92	6.5	0.2	0.9	0.4	0.7	2.2	10.8	0.3	0.6	1.2	1.8
K3_2449	467				0.2	0.2		0.8		0.2	59.71	5.8	0.3	0.8	0.7	0.7	2.5	9.0	0.2	0.6	1.0	1.8
K3_2450	469	-4.66	-13.36		0.3	0.1	0.1	0.0	0.2	1.0	48.89	9.1	0.6	0.7	0.1	0.2	1.7	7.2	0.2	1.3	1.8	1.8
K3_2451	471				0.3	0.0		0.3		0.1											0.9	
K3_2452	473			-29.8	0.2	0.2	0.3	0.4	0.3	0.7	53.90	6.9	0.3	1.1	1.1	0.5	3.0	8.1	0.2	0.8	1.0	1.8
K3_2453	475				1.0	0.1		0.8		0.2											0.9	
K3_2	477	-5.2	-12.		0.6	0.1	0.1	0.3	0.3	0.3	56.21	7.4	0.6	1.1	0.4	0.4	2.5	8.3	0.2	0.9	1.6	1.8

54		8	59																						
K3_2559	479				0.3	0.0		0.1		0.0	47.33		-0.7	0.1	7.9	0.4	0.9	0.7	0.4	2.3	8.6	0.2	0.9	1.8	1.8
K3_2561	481	-6.47	-13.66		0.4	0.2	0.2	0.2	0.4	0.7	60.77				5.7	0.2	0.4	0.3	0.5	1.5	8.1	0.2	0.7	2.2	1.8
K3_2570	490				0.5	0.2		0.1		2.8	64.81				6.3	0.4	0.9	0.6	0.4	2.3	6.9	0.2	0.9	2.5	1.8
K3_2580	500	-2.97	-13.46		0.8	0.2	0.2	0.0	0.2	1.9	43.93				5.8	0.3	0.7	0.3	0.2	1.5	6.7	0.2	0.9	3.1	1.8
K3_259	536.5			-31.0	0.2	0.3		0.4		0.7	29.16	0.12	0.1	7.8	4.2	0.3	0.3	0.0	1.4	2.0	6.0	0.2	0.7	3.7	1.8
K3_260	538				0.6	0.2		0.3		0.8														0.9	1.8
K3_261	540	-5.96	-13.62		0.5	0.2	0.2	0.6	1.5	0.2	36.31	-0.65	-1.6	0.4	5.3	0.3	0.3	0.1	1.8	2.5	8.1	0.2	0.7	1.9	1.8
K3_262	542				0.4	0.1		0.8		0.1	45.22				5.0	0.3	0.3	0.0	0.9	1.6	6.9	0.2	0.7	2.1	1.8
K	5				0	0	0	0	0.	0	41				6	0	0	0	0	1	8	0	0	1	1

3_263	42				.1	.1	.1	.1	2	.6	.78				.1	.3	.6	.2	.3	.4	.4	.2	.7	.2	.8
K3_264	544			-30.8	0.9	0.3		0.0		115.1	39.54				6.7	0.3	0.5	0.1	0.6	1.5	7.3	0.2	0.9	2.8	1.8
K3_265	546	-4.96	-12.91		1.0	0.2	0.2	0.7	0.9	0.3	35.82				6.7	0.3	0.5	0.1	1.2	2.1	8.1	0.2	0.8	1.6	1.8
K3_266	548				0.3	0.2		0.6		0.3	59.22				6.3	0.3	0.4	0.0	0.7	1.5	7.8	0.2	0.8	2.3	1.8
K3_267	550	-3.67	-13.82		0.3	0.1		0.4		0.7	49.80	-0.86	0.1	0.2	6.5	0.4	0.5	0.1	0.8	1.8	8.0	0.2	0.8	1.7	1.8
K3_268	553			-30.7	0.5	0.3	0.1	0.4	1.4	0.2	50.92				7.5	0.4	0.5	0.1	1.6	2.7	8.0	0.2	0.9	2.2	1.8

*Measured using XRF. Calibrated using Ahms et al. (2017). STD=0.10 wt%

Highlights in Scheller et al:

1. Fe-based redox proxies indicate anoxic bottom water conditions in the Arena Fm transiting from euxinic to ferruginous.
2. Super-heavy S isotope compositions are characteristic of the Cryogenian interglacial.
3. Mo-TOC correlations of the euxinic samples indicate a highly restricted basin
4. Mo concentrations and isotopes in three contemporaneous basins suggest the global oceans were in a highly anoxic state.
5. By inference, deglaciation did not drive ocean oxygenation.